DEGREE PROJECT IN MECHANICAL ENGINEERING,
SECOND CYCLE, 30 CREDITS
STOCKHOLM, SWEDEN 2020

Methods to Predict Hull Resistance in the Process of Designing Electric Boats

ELIN LINDBERGH

FELICIA AHLSTRAND

KTH ROYAL INSTITUTE OF TECHNOLOGY
SCHOOL OF ENGINEERING SCIENCES

Methods to Predict Hull Resistance in the Process of Designing Electric Boats
Swedish title: Metoder för att Uppskatta Skrovmotståndet i Designprocessen för Elektriska Båtar

ELIN LINDBERGH, FELICIA AHLSTRAND

TRITA: TRITA-SCI-GRU 2020:185

Degree Project in Naval Architecture, Second Cycle, 30 credits
Course SD271X
Stockholm, Sweden, 2020

Supervisors: Hans Liwång, KTH
Johannes Roselius, X Shore
Examiner: Jakob Kuttenkeuler, KTH

Center for Naval Architecture
School of Engineering Sciences
KTH Royal Institute of Technology
SE-100 44, Stockholm
Sweden
Telephone: +46 8 790 60 00

Host company: X Shore

Abstract

Combustion engines in boats cause several environmental problems, such as greenhouse gas emissions and acidification of oceans. Most of these problems can be reduced by replacing the combustion engines with electric boats. The limited range is one of the main constraints for electric boats, and in order to decrease the energy consumption, applicable resistance prediction methods are necessary in the hull design process. X Shore, which is a start-up company in the electric boat sector, lacks a systematic way of predicting resistance in an early design phase.

In this study, four well-known methods - CFD, Holtrop & Mennen, the Savitsky method and model test - have been applied in order to predict resistance for a test hull. The study is limited to bare hull resistance and calm water conditions. CFD simulations are applied using the software ANSYS FLUENT 19.0. The simulations were based on the Reynolds Average Navier-Stokes equations with SST k-ω as turbulence model together with the volume of fluid method describing the two-phased flow of both water and air surrounding the hull. The semi-empirical methods, Holtrop & Mennen and the Savitsky method, are applied through a program in Python 3, developed by the authors. The results from each method have been compared and since model tests have been conducted outside of this study, the model test results will serve as reference. To evaluate the methods, a number of evaluation criteria are identified and evaluated through a Pugh Matrix, a systems engineering tool.

Holtrop & Mennen predicts the resistance with low accuracy and consistency, and the error varies between 2.2% and 70.6%. The CFD simulations result in acceptable resistance predictions with good precision for the speeds $4 - 6$ knots, with an average deviation of the absolute values as 12.28% which is slightly higher than the errors found in previous studies. However, the method shows inconsistency for the higher speeds where the deviation varies between 1.77% and -43.39%. The Savitsky method predicts accurate results with good precision for planing speeds, but also for the speeds 7 and 8 knots. The method is under-predicting the resistance for all speeds except for 7 knots, where the total resistance is 10.7% higher than for model tests. In the speed range $8 - 32$ knots, the average error is an under-estimation of 17.58%. Furthermore, the trim angles predicted by the Savitsky method correspond well with the trim angles from the model test.

In conclusion, the recommendation to X Shore is to apply the Savitsky method when its applicability criteria are fulfilled, and CFD for the lowest speeds, where the Savitsky method is not applicable.

Sammanfattning

Förbränningsmotorer i båtar orsakar flera miljöproblem, som exempelvis utsläpp av växthusgaser och försurning av hav. De flesta av dessa problem kan minskas genom att ersätta båtar med förbränningsmotorer med elbåtar. Den begränsade körsträckan är en av de största begränsningarna för elbåtar, och för att minska energiförbrukningen behövs metoder för att uppskatta motståndet under designstadiet. X Shore, ett startup-företag i elbåtsbranchen, saknar ett systematiskt tillvägagångssätt för att uppskatta motstånd i tidiga skeden i designprocessen.

I den här studien har fyra välkända metoder - CFD, Holtrop & Mennen, Savitsky-metoden och modelltester - applicerats för att uppskatta motståndet hos ett testskrov. Studien är begränsad till ett skrov utan bihang och lugnvattenmotstånd. CFD-simuleringar har gjorts i mjukvaran ANSYS FLUENT 19.0. Simuleringarna är baserade på Reynolds Average Navier-Stokes ekvationer och turbulensmodellen SST $k-\omega$ har använts tillsammans med metoden *volume of fluid* som beskriver flödet av både vatten och luft runt skrovet. De semi-empiriska metoderna, Holtrop & Mennen och Savitsky-metoden, har applicerats genom ett program i Python 3 som utvecklats av författarna. Resultaten från alla metoder har jämförts, och eftersom modelltester genomförts på detta skrov tidigare har de resultaten använts som referensvärden. Ett antal kriterier har identifierats och en Pugh-matris har använts för utvärdering av metoderna.

Holtrop & Mennen uppskattar motståndet med låg noggrannhet och precision, felen varierar mellan 2.2% och 70.6%. CFD-simuleringarna ger acceptabla resultat av motståndsberäkningarna för hastigheterna $4-6$ knop, med ett genomsnittligt absolut fel på 12.28% vilket är något högre än avvikelserna presenterade i tidigare studier. För högre hastigheter uppvisar metoden lägre precision där avvikelsen varierar mellan 1.77% och -43.39%. Savitsky-metoden ger resultat med hög noggrannhet och god precision för planingshastigheter, men även för hastigheterna 7 och 8 knop. Metoden underskattar motståndet för alla hastigheter förutom för 7 knop där motståndet är 10.7% högre än för modelltesterna. I hastighetsintervallet $8-32$ knop är det genomsnittliga felet en underskattning på 17.58%. Vidare överensstämmer trimvinkeln från Savitsky-metoden bra med resultaten från modelltesterna.

Sammanfattningsvis rekommenderas X Shore att använda Savitsky-metoden när dess kriterier för tillämplighet är uppfyllda och CFD för de lägsta hastigheterna när Savitsky-metoden inte är tillämpbar.

Acknowledgements

This Master's thesis is the final project of the Master's program in Naval Architecture at KTH Royal Institute of Technology and has been carried out at X Shore. We would like to thank the entire X Shore team, and especially our supervisor Johannes Roselius, for helping us, giving us advice and making us feel welcome at the company. Secondly, we want to thank Adam Persson at SSPA for giving us useful advice regarding CFD simulation of planing hulls.

We would also like to express our gratitude to our supervisor at KTH, Hans Liwång, for continuous feedback and support during this semester. Finally, special thanks to Matz Ahlstrand for providing us with a computer that made it possible to finalize our CFD simulations, and to Michael Dellstad for the never-ending IT support.

Thank you.

Elin Lindbergh and Felicia Ahlstrand
Stockholm, June 2020

Work distribution

The authors have contributed equally to the project and worked both independently and in collaboration. The authors have shared the responsibility for the report and its structure and content. Both authors have contributed equally to the sections: 1.2 Purpose and objectives, 1.3 Scope, 1.4 Method, 1.5 Report structure, 2. Ship theory, 5. Evaluation of methods, 6.5 Comparison, 6.6 Evaluation, 7. Discussion and Conclusion and 8. Future work.

Elin Lindbergh has written section 1. Introduction, 1.1 Background, 3. Semi-empirical and empirical methods for ship design and 6.1 Results from previous studies. Elin Lindbergh was responsible for the Savitsky method, including developing the Python script, determining input values, obtaining results and writing section 6.3 Savitsky in the report and associated appendices. Elin Lindbergh converted all Python scripts in this project to executable programs and has also performed CFD simulations.

Felicia Ahlstrand was responsible for Holtrop & Mennen, including developing the Python script, determining input values, obtaining results and writing section 6.2 Holtrop & Mennen in the report and associated appendices. Felicia Ahlstrand has performed most of the CFD simulations and has written section 4. Computational fluid dynamics for ship design and 6.4 CFD.

Contents

Acronyms

Acronyms	Expansions
CAD	Computer aided design
CFD	Computational fluid dynamics
DNS	Direct numerical simulation
DOF	Degrees of freedom
HIRC	High resolution interface capturing scheme
LCB	Longitudinal center of buoyancy
LCG	Longitudinal center of gravity
NM	Nautical miles
RANS	Reynolds Average Navier-Stokes
SST	Shear stress transport
UDF	User defined function
VCG	Vertical center of gravity
VOF	Volume of fluid

Nomenclature

Dimensionless Numbers

Symbol	Description
$(1+k)$	Form factor
ΔC_F	Roughness allowance coefficient
C_f	Friction coefficient
C_V	Speed coefficient
C_{AA}	Air resistance coefficient
C_F	Viscous friction coefficient
C_T	Total resistance coefficient
C_W	Wave-making and wave-breaking resistance coefficient
F_n	Froude number
Re_L	Reynold's number based on the length between perpendiculars
Re_Λ	Reynold's number based on the mean wetted length

Greek Symbols

Symbol	Description
α	Scale factor
β	Deadrise angle
Δ	Displacement mass
ϵ	Angle between keel and propeller shaft
η_D	Propulsion efficiency
η_G	Gearbox efficiency
η_H	Hull efficiency
η_M	Motor efficiency
η_O	Open water propeller efficiency
η_R	Relative rotary efficiency
Λ	Wetted length-beam ratio
∇	Displacement volume
ν	Kinematic viscosity
ρ	Density
τ	Trim angle
τ_w	Wall shear stress

Roman Symbols

Symbol	Description
ΔR	Resistance increase from propeller
Δt	Time step
A_M	Midships cross sectional area
B	Beam
B_m	Model beam
D	Draught at $L_{PP}/2$
d	Water depth
D_m	Model draught
E_B	Battery capacity
f	Distance between propeller shaft and center of gravity
F_T	Propeller thrust force
g	Gravitational acceleration
k_{SM}	Sea margin
L_C	Wetted chine length
L_K	Wetted keel length
L_{OA}	Length overall
L_{PPm}	Model length between perpendiculars
L_{PP}	Length between perpendiculars
L_{WL}	Length on waterline
m	Weight of the boat
P_E	Bare hull power
P_M	Motor power
P_S	Required power
r	Range
R_A	Model-ship correlation resistance
R_B	Additional pressure resistance of bulbous bow
R_F	Frictional resistance
R_T	Total resistance
R_W	Wave-making and wave-breaking resistance
R_{APP}	Resistance of appendages
R_{TR}	Additional pressure resistance of immersed transom stern
S	Wetted surface

t_d	Thrust deduction factor
U	Ship velocity
U_A	Incident propeller velocity
u_*	Friction velocity
U_M	Model velocity
W	Towing tank width
w	Wake fraction
y	Distance
y^+	Dimensionless wall distance

1. Introduction

In 2018, Swedish leisure boats emitted 176 200 tonnes of carbon dioxide equivalent, which corresponds to approximately a third of the emissions from domestic flights in Sweden [1]. Sweden aims to have net-zero greenhouse gas emissions by 2045 at the latest [2], and to meet that goal, a transition from fossil fuels to more sustainable options in the boating sector is inevitable.

Besides the greenhouse gas emissions, boats with traditional combustion engines cause underwater noise, which is known to have a negative impact on marine life, and emit other pollutants, e.g. nitrogen and sulfur oxides that contribute to eutrophication and acidification [3]. By using electric boats, both the emissions and underwater noise pollution can be reduced.

One of the main issues with electric boats is the range, which is limited by the battery capacity. In order to increase the range there are two options: add more batteries, or decrease the energy consumption when driving the boat. Since adding batteries increases both weight and cost, lowering the energy consumption is the more desirable option. This can be achieved by designing a hull with lower resistance.

1.1 Background

The process of designing a ship can be divided into three phases; concept design, contract design and detailed design. How long time that is spent on each phase, as well as how deeply different aspects are studied, depends on ship type and size and varies for each case. However, having a systematic approach when designing a ship is of importance, since it ensures that no aspect is forgotten or dealt with at the wrong time. [4] Moreover, it is important to have a clear priority of the goals of the design. The ship owner must decide if the ship should be optimized with respect to functionality, efficiency, maintenance, environment, or another design aspect, as well as the importance of each aspect. [5]

The first phase, the concept design, is considered the most important phase. The naval architect, together with the project owner, will clarify the environment that the ship will operate in based on the intended route. A basic design, including speed requirements, size and type of hull will also be set to ensure that the owner's requirements will be met. Another purpose of the concept phase is to determine if it is possible to meet the owner's objectives without exceeding the budget. It is therefore important to spend a sufficient amount of time in this design stage, so that a realistic cost estimation can be made and expensive changes in later phases can be avoided. [4] This design phase is an iterative process, resulting in a chosen hull design that will be further developed in the next phase [5]. Figure 1 presents Molland's [5] flowchart of this stage.

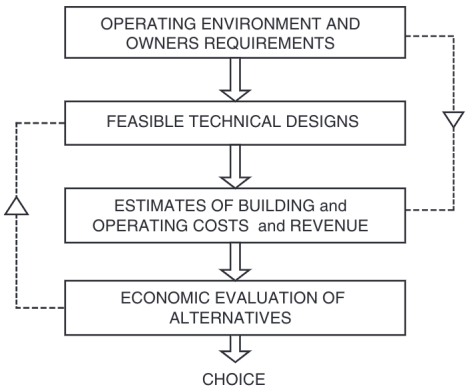

Figure 1: The iterative process of the first design phase [5].

The next phase is the contract design. This phase can either be performed by the same engineers as in the first phase, or by a shipbuilder or a third party. During this stage, performance characteristics will be predicted, for example with CFD simulations. The systems and subsystems necessary in order for the ship to function as intended are identified, sized and positioned. The layout of the ship is determined, in such detail that it can be guaranteed that all necessary equipment and functions fit and that the cargo capacity is sufficient. [4] Since most design aspects of a ship, e.g dimensions, speed and stability, are dependent on each other, the contract design phase is an iterative process [5]. Decisions that are made during this phase should be documented and it should be controlled that the one who made the decision had the authority to do so [4].

The outputs from the contract design will be the input to the final phase, which is the detailed design. The purpose of this phase is to provide the ship builder with enough information, and on such a detailed level, so that the ship can be produced. Additionally, the detailed design should specify the tests necessary in order to determine if the ship meets regulations and the owner's requirements. [4]

The traditional way of designing a ship is to base the design on an already existing ship of the same type. The naval architect can then improve the design, based on known issues in the already existing ship. Identifying differences between the new and the existing ship, such as an increased need of cargo capacity or higher speed requirements, will also affect the design, as well as new regulations that are to be met. If the new design deviates too much from already existing ship types, the design process will be more iterative. With no existing ship to base the design on, it is important to identify the ship's functions, capabilities and attributes. The functions can be to float and move, and the capabilities will ensure that the functions are achieved, for instance by the capability to operate in a certain speed. The attributes are the features that the naval architect designs into the ship in order to support the capabilities. Stability, manoeuvrability and strength are examples of attributes, and several attributes might be necessary for one capability. [4]

1.1.1 The design process at X Shore

X Shore is a Swedish company that designs and manufactures fully electric leisure boats. The current models in the X Shore family are the 6 m long Eelord and the 8 m long Eelex. X Shore embraces the long tradition of maritime craftsmanship and with new technology, innovative research, smart design and sustainable materials their aim is to discard the usage of fossil fuels [6].

The design process at a company like X Shore is affected by the fact that it is a small start-up company with limited resources and competence. The main design objectives for X Shore are to combine sufficient range with the silence from an electric motor. As a start-up company, X Shore is still in the progress of defining the typical X Shore hull, and consequently, major design changes are made when designing new hulls. Hence, X Shore has no existing hulls to base the designs on. The innovative and nontraditional design process result in a more iterative process where the functions, capabilities and attributes need to be identified.

During the concept design, an external hull designer works closely together with a design team at X Shore. The hull designer possesses valuable knowledge and experience, and the X Shore team ensures that the brand identity is kept as well as requirements are met. The process is iterative, with design reviews where the hull designer presents a draft design, and the X Shore team gives feedback and suggests modifications.

In the contract design phase, engineers at X Shore identify, size and position necessary systems and subsystems. Previously, external consultants have been involved to a small extent, in order to predict performance characteristics. However, X Shore has no systematic way of predicting performance and thus, no methods to evaluate the impact of design changes.

The detailed design is carried out by X Shore's engineers. X Shore also have the competence to specify what tests that need to be conducted and how to ensure that regulations and require-

ments are met. While both the concept design and detailed design work out well, there are some deficiencies in the contract design regarding performance prediction. For future designs, X Shore wants to develop their design process so that performance predictions can be made in-house to the greatest extent possible.

As energy consumption is one of the main constraints for the range of the boats, one of the biggest challenges when designing a new hull for the X Shore family is to reduce the resistance for both displacing and planing speeds.

1.1.2 Methods to predict resistance

The resistance forces acting on a hull are caused by characteristics of both the water and the hull. There are different approaches to predict the resistance in the design phase. Well-known methods are computational fluid dynamics (CFD), model tests, the Savitsky method and Holtrop & Mennen. CFD is applied in most disciplines involving a flowing fluid, including the ship industry. The tool is especially useful when there is a complex fluid flow involved [7]. Since the time and cost required for CFD are lower than for model test, the use of the tool in ship design is increasing. The difficulties with CFD in ship design have previously been to accurately model a free surface. However, the models have improved significantly and the tool can now yield good results. [8]

Model tests are empirical tests using scale models in towing tanks. Model tests provide more accurate results than CFD, but to a much higher cost [7]. The Savitsky method and Holtrop & Mennen are semi-empirical methods for planing and displacement hulls, respectively. These two methods are easily implemented [9] and less time and cost consuming in comparison to CFD and model tests. The drawback is however that these two methods are based on simple hull shapes and therefore restricted to shapes similar to these [10]. For more complex hull shapes another tool is required.

1.2 Purpose and objectives

Since methods to predict performance characteristics are absent in X Shore's design phase, the aim of this project is to provide X Shore with a systematic approach to predict resistance of new hull designs. Four well-known methods - CFD, Holtrop & Mennen, the Savitsky method and model tests - will be evaluated and compared with each other in order to find the methods that are most suitable for X Shore. To enable comparisons, a set of evaluation criteria will be identified. It will also be clarified when and how to apply the suggested methods. As the goal for X Shore is to lower the energy consumption, the results from the resistance predictions will be presented as the corresponding range for each speed.

1.3 Scope

The study is limited to evaluating and performing CFD simulations, Holtrop & Mennen and the Savitsky method on the test hull Eelex 2020 developed by X Shore, see figure 2.

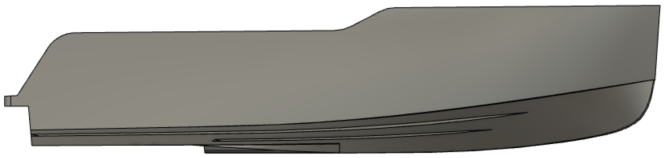

Figure 2: Eelex 2020.

Model tests will be investigated, but not conducted. Instead, the results from the other methods will be compared to existing results from model tests made on the test hull. To enable comparisons between the methods, resistance predictions are made on a bare hull, meaning that no appendages, e.g. propellers or rudders, are included. Moreover, the predictions are made for calm water conditions. The main characteristics of Eelex 2020 are presented in table 1.

Table 1: Main characteristics of Eelex 2020.

	Symbol	**Value**	**Unit**
Length overall	L_{OA}	7.955	m
Length between perpendiculars	L_{PP}	7.489	m
Breadth	B	2.550	m
Draught at $L_{PP}/2$	D	0.399	m
Weight	m	2600	kg
Battery capacity	E_B	120	kWh

1.4 Method

Initially, a literature study is performed in order to get better understanding of the characteristics that will be analyzed, the methods for resistance predictions and the guidelines on how to apply these methods. To evaluate the methods, the methods are applied on Eelex 2020 and compared considering a set of identified criteria. The evaluation and comparison study is the basis of the conclusion regarding when and how to systematically apply the suggested approach.

1.5 Report structure

In chapter 2, planing hull theory and the resistance forces acting on a hull are explained together with theory regarding power requirements and efficiency. The semi-empirical Savitsky method and Holtrop & Mennen are presented in chapter 3. The empirical model test are presented in the same chapter. Chapter 4 explains the theory behind CFD and guidelines in how to perform a simulation on a hull. In chapter 5, the evaluation criteria are identified and the results presented in chapter 6 contains of a step by step summary in how to apply the suggested methods followed by an evaluation based on the identified criteria. Finally, when to apply the different approaches are discussed and concluded in chapter 7, and suggestions for future work can be found in chapter 8.

2. Ship theory

The purpose of this chapter is to provide the reader with necessary ship theory. The first section introduces the theory of hull resistance and planing hulls, and is followed by a section describing efficiency and power requirements.

2.1 Hull resistance

According to Almeter [11] hulls can be divided into three different types: pre-planing, semi-planing and fully planing hulls. The Froude number can be used as an indication of the type of a hull, and is defined as

$$F_n = \frac{U}{\sqrt{gL_{PP}}} \tag{1}$$

where U is the speed of the boat, L_{PP} is the length between perpendiculars and g is the gravitational acceleration. While there is no clear limit [12], a general rule is that $F_n < 0.4$ indicate a pre-planing hull, also known as displacement hull, and $F_n > 1.0$ indicate a fully planing hull. Between 0.4 and 1.0 the hull is assumed to be semi-planing. [13] Thus, all hulls are displacing in low speeds.

Figure 3 presents both a displacement and a planing hull and the main difference between these is the pressure generated forces acting on the hull. There are two different types of pressures involved; hydrostatic and hydrodynamic pressure, acting through a point called center of pressure. For a displacement hull the hydrostatic pressure, i.e. buoyancy, is predominant [13]. The buoyancy is equal to the weight of the volume of fluid that a hull displaces. As the speed increases, the importance of the buoyancy decreases and the hull is mainly supported by hydrodynamic pressure. The hydrodynamic pressure is generated by the flow around the hull and is proportional to the speed squared. [12] The vertical components of the hydrodynamic pressure lift the boat out of the water, which results in planing, while the longitudinal components cause resistance [14].

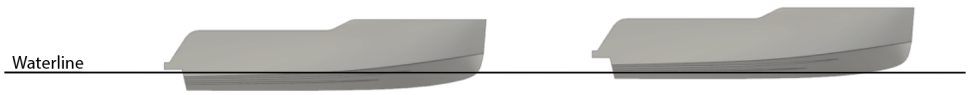

Figure 3: The hull to the left is displacing, while the hull to the right has reached planing.

Resistance is a force acting on the hull in the opposite direction of the motion, i.e. in the horizontal direction. The components of the total resistance can be divided in different ways, whereof one is presented in figure 4. Wave resistance and viscous pressure resistance are caused by the longitudinal components of the hydrodynamic pressure, and is thus increasing with the speed [14]. The viscous friction, also called drag force, is caused by the friction between the hull and the water as the boat is moving [15]. For low speeds, where the hull is mainly supported by hydrostatic pressure, the total resistance is dominated by the frictional resistance. The pressure resistance increases with increasing speeds, and wave resistance and friction resistance are dominating for planing hulls. [9]

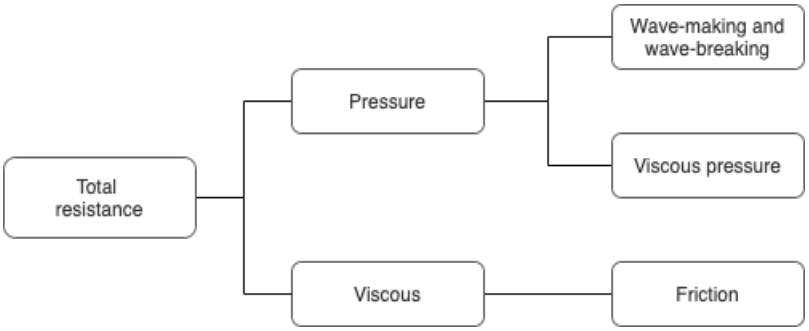

Figure 4: The components of the total resistance.

The total resistance is defined as

$$R_T = \frac{1}{2}\rho U^2 C_T S \tag{2}$$

where ρ is the density of the fluid, U is the speed of the boat and S is the wetted surface of the hull. C_T is a dimensionless total resistance coefficient defined as

$$C_T = (1+k)C_F + C_W + \Delta C_F + C_{AA} \tag{3}$$

where $(1+k)C_F$ is the viscous friction and form drag coefficient, C_W is the wave-making and wave-breaking resistance coefficient, ΔC_F is the roughness allowance coefficient and C_{AA} is the air resistance coefficient. Resistance from appendages are not included in equations 2 and 3, but can be added as separate terms. [9]

In order to predict resistance for a boat, variables that define the basic dimensions and loading of the hull are of interest. According to Almeter [11] these variables are speed and displacement, length and beam, deadrise angle and longitudinal center of gravity (LCG). The deadrise angle is the angle between the keel and the horizontal plane, see figure 5a. A large deadrise angle reduces the lift force, which in turn increases the wetted surface, resulting in higher resistance. Consequently, a small deadrise is desirable in order to minimize the resistance. However, reducing the deadrise angle results in increased slamming, which is undesirable. [14] Thus, determining the appropriate deadrise when designing a hull is a balance between resistance and slamming forces.

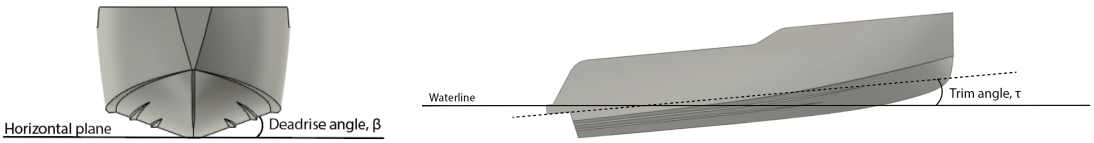

(a) The deadrise angle β.

(b) The trim angle τ.

Figure 5: The deadrise angle β is shown to the left and the trim angle τ is shown to the right.

LCG is the longitudinal position of the center of gravity in the boat, which affects the trim angle, i.e. the angle between hull and the water surface, see figure 5b. The trim angle affects the wetted surface and therefore also the resistance [14]. For displacement hulls and semi-planing hulls, a typical position for the LCG is around $40\% - 45\%$ and $33\% - 45\%$ of the chine length forward of the transom, respectively. Planing hulls, designed to be lifted up from the water to decrease the displacement volume, tend to have the LCG placed at $25\% - 35\%$ of the chine length from the transom. [11]

In displacement speeds, the draught and trim of the hull, i.e. the running attitude, is assumed to be the same as in zero speed, since the hull is mainly supported by hydrostatic pressure and both LCG and the center of pressure is constant. As the speed increases, the hydrodynamic pressure will lead to a decrease in submerged volume and draught, and consequently, the center of pressure will move. Since LCG is constant, the change of center of pressure will cause varying trim angles. The running attitude influences the wetted surface, which in turn affect the resistance, and it is therefore important to capture the effects from changes in trim and draught when calculating resistance in semi-planing and planing speeds.

2.2 Efficiency

The power requirements for a ship in calm water can be expressed as

$$P_S = \frac{P_E}{\eta_D} \tag{4}$$

where P_E is the bare hull power and η_D the propulsion efficiency. The propulsion efficiency can be expressed as

$$\eta_D = \eta_O \eta_R \eta_H \tag{5}$$

where η_O is the open water propeller efficiency, η_R is relative rotary efficiency, approximately equal to 1. The hull efficiency, η_H, is defined as

$$\eta_H = \frac{1 - t_d}{1 - w} \tag{6}$$

where t_d is the thrust deduction factor and w is the wake fraction:

$$t_d = \frac{\Delta R}{F_T} \tag{7}$$

$$w = 1 - \frac{U_A}{U} \tag{8}$$

ΔR is the increased resistance due to the propeller, F_T is the propeller thrust force, U_A is the incident propeller velocity and U is the ship velocity. For vessels with one propeller, the thrust deduction factor t_d and the wake fraction w can be estimated as

$$w = 0.5 C_B - 0.05 \tag{9}$$

$$t_d = 0.6w \tag{10}$$

and for vessels with two propellers as

$$w = 0.55 C_B - 0.20 \tag{11}$$

$$t_d = 1.25w \tag{12}$$

C_B is the block coefficient, defined as

$$C_B = \frac{\nabla}{BDL_{PP}} \tag{13}$$

where ∇ is the displacement volume, B is the beam, D is the draught and L_{PP} is the length between perpendiculars. It should be noted that the propulsion efficiency η_D can exceed 1, since η_H usually is larger than 1. To capture the effects from waves and winds, a sea margin of 15 % is usually added to the power requirements in equation 4. [9]

If there is a gearbox between the motor and the propeller shaft, further energy losses occur. The required output power from the motor, P_M can then be expressed as

$$P_M = \frac{k_{SM} P_S}{\eta_G} \tag{14}$$

where k_{SM} is the sea margin and η_G is the efficiency of the gearbox. The electric motor used in the X Shore boats has a nominal speed of 4400 rpm and a maximum speed of 12000 rpm [16], but since that speed is too high for the propeller, a gearbox is needed. When the motor power P_M is known, the range r can be calculated by

$$r = \eta_M \frac{E_B}{P_M} U \tag{15}$$

where η_M is the motor efficiency and E_B is the energy in the battery, i.e. the battery capacity.

3. Semi-empirical and empirical methods for ship design

This chapter presents three widely used methods for resistance prediction in ship design; the semi-empirical methods by Savitsky and Holtrop & Mennen, and empirical model tests. If used, these methods should be applied in the contract design phase.

3.1 Holtrop & Mennen

Holtrop & Mennen is a method based on empirical equations, derived from a large number of model test results. It is considered one of the most accurate methods for predicting resistance in the design phase. However, since the equations are derived from model tests performed in the 1970s and 1980s, the hulls might differ from today's designs and the equations might give less accurate results. [17] The method is intended for resistance prediction for displacement hulls and the range of applicability is limited by following criteria [15]:

$$F_n < 0.45$$
$$0.55 \leq C_P \leq 0.85$$
$$3.9 \leq \frac{L}{B} \leq 9.5$$

C_P is the prismatic coefficient defined as [9]

$$C_P = \frac{\nabla}{L_{PP} A_M} \tag{16}$$

where ∇ is the displacement volume, L_{PP} is the length between perpendiculars and A_M is the midship cross sectional area.

The total resistance R_T is defined as

$$R_T = (1+k)R_F + R_{APP} + R_W + R_B + R_{TR} + R_A \tag{17}$$

where R_F is the frictional resistance according to the ITTC formulation [18], $(1+k)$ is a form factor describing the viscous resistance of the hull form in relation to R_F, R_{APP} is the resistance of appendages, R_W is the wave-making and wave-breaking resistance, R_B is additional pressure resistance of bulbous bow near the water surface, R_{TR} is additional pressure resistance of immersed transom stern and R_A is the model-ship correlation resistance. Detailed descriptions on how to determine the different resistances can be found in Appendix A. [19]

3.2 Savitsky method

The Savitsky method is widely used to evaluate resistance for planing hulls. It is based on empirical prismatic equations and assumes that the part of the hull in contact with water when planing has a constant cross-section. [11] By determining the equilibrium trim angle through iteration, the method takes the running attitude of the hull into account when prediction the resistance. According to Savitsky [20] the total hydrodynamic drag of a planing hull can be described as

$$D = \Delta tan(\tau) + \frac{\varphi U^2 C_f \Lambda B^2}{2cos(\beta)cos(\tau)} \tag{18}$$

where Δ is the displacement mass, τ is the trim angle, U is the hull speed, B is the beam and β is the deadrise angle.

φ is defined as

$$\varphi = \frac{\gamma}{g} \tag{19}$$

where γ is the specific weight of water and g is the gravitational acceleration. Λ is the mean wetted length-beam ratio, defined as

$$\Lambda = \frac{L_K + L_C}{2B} \tag{20}$$

where L_K is the wetted keel length, L_C the wetted chine length and C_f is a friction coefficient. Savitsky [20] refers to the friction coefficient formulated by Schoenherr, which was the standard friction coefficient from 1947. However, this formulation had certain deficiencies and ITTC developed an improved formulation in 1957. [21] The ITTC formulation [22] will be used in this project and is expressed as

$$C_f = \frac{0.075}{[log_{10}(Re_\Lambda) - 2]^2} \tag{21}$$

where Re_Λ is the Reynold's number based on the mean wetted length, defined in Savitsky [20] as

$$Re_\Lambda = \frac{U\Lambda B}{\nu} \tag{22}$$

where ν is the kinematic viscosity of the water. Even though the friction coefficient C_f was developed for traditional hulls, and consequently may not give accurate results for unconventional hull shapes, it is widely used. [23] The method is applicable when following criteria are met [20]:

$$0.6 \leq C_V \leq 13$$

$$2^\circ \leq \tau \leq 15^\circ$$

$$\Lambda \leq 4$$

where C_V is a speed coefficient defined as

$$C_V = \frac{U}{\sqrt{gB}} \tag{23}$$

Detailed descriptions on how to calculate the resistance with the Savitsky method can be found in Appendix B.

3.3 Model tests

Model tests are performed with a scale model of the hull in a towing tank. The model should have the same Froude number as the full scale hull in order to obtain useful results, which means that the model speed should be adjusted according to Froude's model law:

$$U_M = \frac{U}{\sqrt{\alpha}} \tag{24}$$

where U_M is the model velocity, U is the ship velocity and α is the scale factor. When the model is towed in the towing tank, resistance, trim and sinkage are measured. Moreover, the water temperature is measured in order to calculate the water's density and viscosity. [9] By measuring the towing force, the resistance can be determined [24].

The model can be tested in two conditions; with and without appendages. When testing without appendages, also known as bare hull, the resistance due to the hull shape is determined. Sometimes a rudder is included in the bare hull test. The purpose of tests with appendages is to determine how

much the appendages affect the total resistance. [24] To obtain as accurate trim measurements as possible, the direction of the towing force should be applied in the longitudinal center of buoyancy (LCB) and in the line of the propeller shaft. [24]

Generally, the bigger the model the better. However, if the model gets too big in comparison to the towing tank, it will affect the velocity field and thus the results. Hence, the following criteria for model length between perpendiculars L_{PPm}, model draught D_m and model beam B_m should be fulfilled:

$$L_{PPm} < d$$

$$L_{PPm} < W$$

$$D_m B_m < \frac{Wd}{200}$$

where d is the water depth and W the width of the towing tank. [9] Model tests have played an important role in traditional ship design, but it is a costly method [8].

4. Computational fluid dynamics for ship design

Computational fluid dynamics (CFD) is the analysis of fluid flows, using numerical methods. CFD can be used to simulate a flow and analyse the interaction between a fluid and an object, e.g. to determine lift or drag, and it can therefore be used to simulate ship hydrodynamics. It is an efficient supplementary technique to costly model tests [8] and it has been demonstrated that a CFD simulation give acceptable accuracy compared to experimental data such as the Savitsky method [25]. If CFD is used in the design process, the simulations are done during the contract design. One of the advantages with CFD for resistance predictions in the early design phase is that modifications of the hull can be done in both a relatively short time and to a relatively low cost, which enables comparisons of results for different hull forms [7]. In this project, ANSYS FLUENT 19.0 has been used and the following chapter will focus on theory relevant to perform a CFD simulation for resistance prediction on a hull using that software.

4.1 Geometry and computational domain

Geometries used in CFD simulations are defined in a computer aided design (CAD) software and then converted to a file format compatible with the CFD software [23].

The orientation of the reference coordinate system, as well as the origin, should be chosen carefully. In order to minimise the risk of errors, the aim is to have the coordinate system aligned with the forces of interest and recommendations are to use the same coordinate system in both the CAD and the CFD software. [23]

For simulations of ship hydrodynamics, the computational domain can be built in several ways. It is important to make it big enough to capture the wake behind the ship, but small enough to save computational cost. According to ITTC guidelines for ship CFD applications [23] the domain is built as a rectangular block around the imported hull surface. To reduce the grid size by half, the port-starboard symmetry can be taken into advantage and only half of the full domain is then computed, using a symmetry boundary condition on the ship's center plane [8][18][25].

The domain should include an inflow and outflow surface, placed sufficiently far away from the ship. The inlet boundary should be placed $1-2L_{PP}$ upstream of the ship and the outlet boundary at $3-5L_{PP}$ downstream of the ship, where L_{PP} is the length between perpendiculars of the hull [26]. Other boundaries of the domain should be placed at least $1L_{PP}$ away from the hull. [23] Figure 6 shows the computational domain.

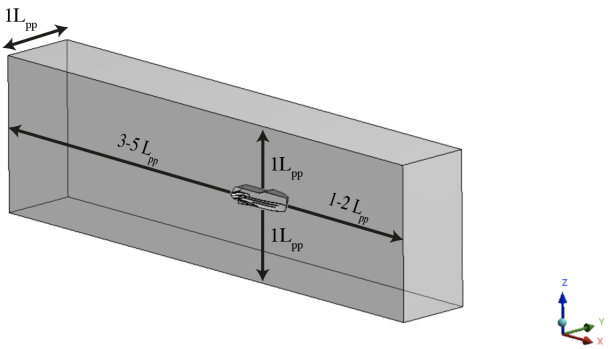

Figure 6: The size of the computational domain.

4.1.1 Boundary conditions

In addition to the symmetry boundary condition on the ship's center plane, boundary conditions for the inflow and outflow should be defined [23]. The inflow boundary is often imposed as a velocity field, and defined as a velocity inlet since the flow is initiated from this boundary [23] and it is suitable for incompressible flows [7]. For the outflow boundary, a pressure outlet with a Neumann condition is recommended [23]. On the hull, a no-slip wall boundary condition is usually applied [7], see figure 7.

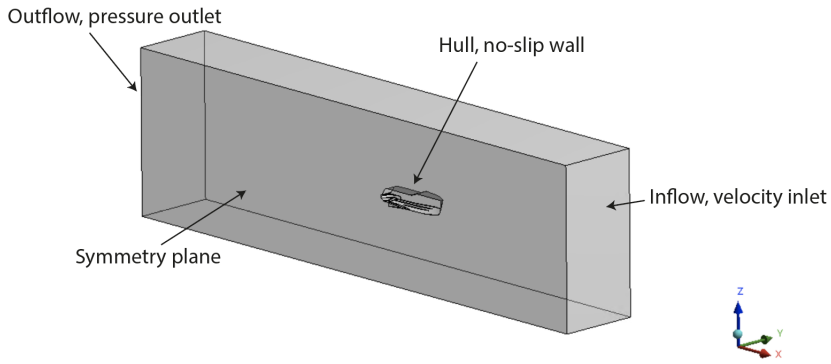

Figure 7: The boundary conditions for the computational domain.

4.2 Mesh

In order to use numerical equations, the domain is divided into smaller cells, called a mesh. The mesh can be built out of structured or unstructured grids. Structured grids for three dimensional domains are build out of hexahedral elements while the unstructured grid cells can have hexahedral, tetrahedral, polyhedral or several other shapes, see figure 8. Unstructured grids are in general slower and have less accuracy than equivalent structured grids. [23] Converting the mesh to polyhedral cells can decrease the overall cell count [27].

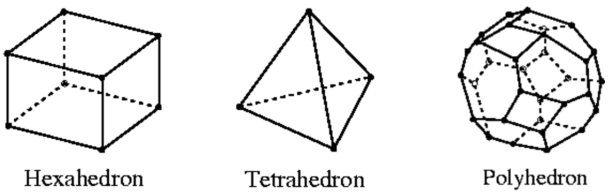

Figure 8: Different shapes of cell elements that can be used to build a mesh.

In order to capture the flow on the free surface with high accuracy, orthogonal grids should be used [23]. Since the waves created on the surface are much longer than they are high, high resolution on the grid in vertical direction is required [28]. To capture this, a cell size in the vertical direction, i.e. along the z-axis should be

$$z = \frac{L_{WL}}{1000} \tag{25}$$

where L_{WL} is the length of the waterline on the hull [28].

4.2.1 Boundary layer

When a fluid and a structure interacts, shear stresses arise on the surface of the structure which creates a boundary layer. When the free stream reaches the structure with a uniform velocity a laminar boundary layer starts to grow at the structure surface. The boundary layer, which affects the velocity profile, grows along the surface and after some distance it goes into a transition region after which the boundary layer becomes turbulent. Close to the surface, the boundary layer will remain laminar and the turbulence will increase further away from the structure surface.

To capture this behavior when simulating a fluid-structure interaction, ANSYS FLUENT uses a dimensionless wall distance to characterize the flow near the structure surface. The dimensionless wall distance is defined as

$$y^+ = \frac{u_* y}{\nu} \tag{26}$$

where y is the distance to the structure surface, ν is the kinematic viscosity and u_* is a friction velocity,

$$u_* = \sqrt{\frac{\tau_w}{\rho}} \tag{27}$$

in which ρ is the water density and τ_w is the wall shear stress defined as [10]

$$\tau_w = \rho\nu \left.\frac{\partial U}{\partial y}\right|_{y=0} \tag{28}$$

Experiments have shown that the near-wall region can be divided into sublayers. The innermost layer, the viscous sublayer, consists of a flow that is almost laminar and where the viscosity dominates and $y^+ \leq 5$. The outermost layer, the log-law layer, is fully turbulent and thus, turbulence dominates. In between these two layers there is a layer called the buffer layer where viscosity and turbulence are equally important and where $5 \leq y^+ \leq 60$. [27]

To properly model the near-wall region, in this case the boundary layer close to the hull, prism layer mesh can be used. This can be done by either using near-wall turbulence models or by using wall functions. Depending on the level of accuracy required, chosen turbulence model and whether wall functions are used or not, the number of grid points can be determined in terms of y^+. Near-wall turbulence models resolve the flow in the laminar sub-layer all the way down to the wall, requiring at least 3 points in the boundary layer. Therefore, it is recommended to use a $y^+ \leq 1$ with an expansion ratio of 1.2 resulting in 20 points within the boundary layer. Wall functions are semi-empirical formulas that without resolving the viscous sub-layer, bridge the solution variables in the turbulent log-law layer and the corresponding quantities on the wall. The first point from the wall is recommended to be within the log-law layer. Thus, the dimensionless wall distance value is recommended to be $30 \leq y^+ \leq 100$ with an expansion ratio of 1.2, resulting in 15 points within the boundary layer. [23]

Choosing y^+ value, i.e. near-wall models or wall functions, is a trade-off between computational effort and accuracy. Near-wall models is a more rational approach, but the highly refined grids can lead to numerical instability making the computations heavy. On the other hand, wall functions are based on two-dimensional flows at zero pressure gradients and the analytical expressions become less valid with increasing pressure gradient. If possible, wall functions should be avoided. [23]

However, once the y^+ is chosen, the distance y of the first point in the boundary layer can be determined as

$$y = \frac{y^+ L_{PP}}{Re_L \sqrt{\frac{C_f}{2}}} \tag{29}$$

where C_f is the friction coefficient and Re_L is the Reynolds number based on the length between perpendiculars, defined as

$$Re_L = \frac{U L_{PP}}{\nu} \tag{30}$$

In regions where high resolution is required, i.e. near the free surface and in the boundary layers, tetrahedral cells should be avoided. Hexahedral or prismatic cells result in better convergence rates and higher accuracy and should therefore be used in regions requiring high resolution. [23]

4.3 Turbulence

The flow around a hull traveling with high speed is a turbulent flow [10]. Turbulent flow, in contrast to laminar flow, is characterised by random and chaotic variations in the flow's velocity and speed, resulting in a three-dimensional flow with vortices [29].

The Navier-Stokes equations are the governing equations for fluid flows consisting of the continuity and the momentum equations. The equation of continuity implies a material balance over a stationary fluid element. The momentum equations, also called the equation of motion, describes the momentum balance which according to Newton's second law requires that the rate of change in momentum on the fluid particle is equal to the force acting on it. [30] Analytical solutions for solving the Navier-Stokes equations for turbulent flows do not exist, so they need to be treated numerically [10]. To solve the equations directly by direct numerical simulation (DNS) which resolve the flow completely, is extremely computationally expensive and time consuming. Therefore, the most common way to simulate turbulent flows is based on the Reynolds Averaged Navier-Stokes (RANS) equations. These are simplified Navier-Stokes equations which are not as accurate as DNS, but requires less computational effort. The idea of RANS equations is to describe the flow as the turbulent viscosity fluctuations separated from the mean flow velocity. The main differences between the original Navier-Stokes equations and the RANS equations is the Reynolds stress term, which introduces the coupling between the turbulent fluctuations and the mean velocity. To model this term is the sole purpose of RANS turbulence modelling and can be modelled by determine a eddy viscosity. To determine this viscosity, and solve the RANS equations, a turbulence model is needed. [30]

The three most commonly used turbulence models are the standard k-ϵ model, the k-ω model and the SST k-ω model. The SST k-ω model is a combination of the standard k-ϵ and k-ω models, which has shown good performance for complex flows. In the boundary layer the k-ω model is used because of its validity in regions of low turbulence, i.e. close to walls. For the free flow, the standard k-ϵ model is used, formulated on k-ω form, since it is a robust model with good predictions for fully turbulent flows. [10] For simulating ship hydrodynamics the SST k-ω model is the most commonly used turbulence model [8][23][25][31]. When using a two-equation turbulence model as the SST k-ω, the time step Δt must be

$$\Delta t \leq 0.01 \frac{L}{U} \tag{31}$$

where L is the length and U is the speed of the boat [23].

4.4 Two-phased flows

The intended simulations contain two fluids, water and air, which need to be simulated as two different phases. This can be done by using the multiphase method in ANSYS FLUENT. The two phases are separated by a free surface which is resolved with the volume of fluid (VOF) formulation and open channel boundary conditions.

The VOF formulation enables modelling of two immiscible fluids and is in general used to compute time-dependent solutions. However, it can also be used for steady-state calculations if the solution is independent of the initial conditions and there are distinct inflow boundaries for the two different phases. [27]

The multiphase method divides the computational domain into two different phases based on where the free surface is placed, see figure 9, and the fluid's characteristics need to be defined. The open channel flow model enables to define the location of the free surface. However the model requires that the open channel boundary condition for the inlet is defined as either pressure inlet or mass flow rate and the outlet as either pressure outlet or outflow boundary. [27] Necessary for simulations with a free surface is also to define the direction and magnitude of the gravitational acceleration g [7].

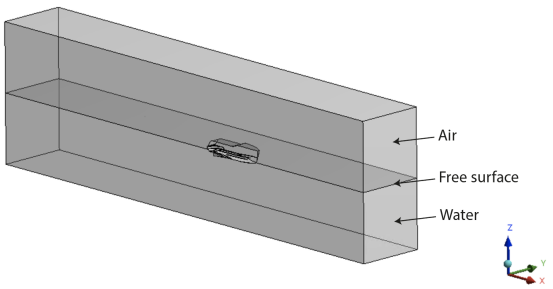

Figure 9: The multiphase method divide the computational domain into two different phases.

4.4.1 Numerical ventilation

A common problem when applying the VOF formulation on planing hulls is a phenomenon called numerical ventilation. The simulated resistance is reduced due to a thin layer of air between the hull and the water, decreasing the friction. Furthermore, the air under the hull might have an impact on the pressure distribution and the trim of the hull, which also affects the resistance [32]. This phenomenon is completely artificial, meaning that it only appears in simulations and not in real situations. Therefore, it is necessary to remove the effect of the numerical ventilation. One way to do this is to use a user defined function (UDF) and loop through every cell in the boundary layer close to hull, and for cells where the volume fraction of air is below a certain limit, it is set to 0 [10]. It is shown that low values of the dimensionless wall distance y^+, first order modelling of the convection terms and large time steps increase the effects of numerical ventilation. Consequently, it is recommended to have $y^+ \approx 30$ and to model the convection term using a second order scheme. [33] Moreover, a modified HRIC scheme decreases the numerical ventilation significantly in comparison with a regular HRIC scheme. [32]

4.5 Fluid-structure interaction

When simulating a hull, it is assumed that the hull will reach an equilibrium, i.e. a steady position and orientation with respect to the free surface, when moving with constant speed. Before reaching this equilibrium, the hull will have a dynamic behaviour where the interaction between the fluid, in this case water, and the structure, which in this case is the hull, needs to be considered. This is

done by solving the equations of motion and rotation of the boat as it is influenced by the forces and moments from the surrounding fluids and gravitational acceleration. [10] The boat can be considered as a rigid body which in general is allowed to move in six degrees of freedom (DOF); translation in three directions and rotation in three directions, along and around the x, y and z axes, respectively. The translation motions are called surge η_1, sway η_2 and heave η_3 along the x, y and z axes, respectively, and around the same axes are the rotational motions called roll η_4, pitch η_5 and yaw η_6, see figure 10. [34]

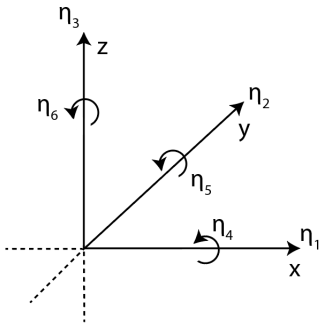

Figure 10: Translation motions surge η_1, sway η_2 and heave η_3 and the rotational motions roll η_4, pitch η_5 and yaw η_6 along and around the x, y and z axes, respectively.

To solve the equations of motion and rotation, ANSYS FLUENT uses a six DOF solver. The solver follows an iterative procedure until the equilibrium is reached and the running attitude is identified. A six DOF solver requires that the mass and the moments of inertia are specified. The six DOF solver is often limited to two DOF, heave and pitch, through a UDF. The UDF is then written to only allow for translation along the z-axis, heave η_3, and rotation around the y-axis, pitch η_5, and is defining the required properties. [10] Heave and pitch are earlier mentioned as changes in draught and trim, which define the running attitude of the ship.

4.6 Dynamic mesh

In order to capture motions in several degrees of freedom when modelling, a dynamic mesh is required. ANSYS FLUENT has three different methods for dynamic meshing: smoothing methods, dynamic layering and remeshing methods. For complex dynamic problems, these methods can be combined. [35] The smoothing methods change the shape of the nodes, while there are no changes in the number of nodes and their connectivity. The remeshing methods collect cells in the mesh that are invalid, e.g. cells with negative volume, and updates the mesh with new cells. If using dynamic layering, a cell layer close to the moving surface can be added or removed, based on the height of the cells next to the moving surface. [36]

4.7 Schemes

The numerical methods in ANSYS FLUENT can be density-based or pressure-based. The density-based solver can either use implicit or explicit numerical methods, where the difference is that the implicit method uses both unknown and known values from neighbouring cells while the explicit only uses known values. [27] When applying the pressure-based solver, two different algorithms are available: a segregated and a coupled algorithm. The coupled algorithm results in a reduced convergence time, but requires a higher computational cost than the segregated algorithm. [36] The pressure-based solver is required when appling the VOF model [27].

Continuous equations need to be discretized in order to be solved numerically. For steady-state flows, spatial discretization is needed. For cases with transient flow, both spatial and temporal

discretizations are required. The spatial discretization in ANSYS FLUENT is done with an upwind scheme, meaning that values in a cell are derived from the cell in the upstream direction, compared to the normal velocity. This can be done with a number of different schemes: first-order upwind, second-order upwind, power-law, and QUICK. The temporal discretization can be done with either implicit or explicit time integration. The implicit time integration is stable regardless of the size of the time steps, but has a higher computational cost than the explicit integration. However, the explicit time integration cannot be used to compute incompressible flows and requires that a density-based explicit solver is used. [27]

According to ITTC [23], the second-order upwind scheme is used in the majority of industrial CFD codes. It is recommended for all convection-diffusion transport equations since it is reasonably accurate and robust. [23]

4.8 Quality

Convergence of the solution, a grid independence study and the dimensionless wall distance y^+ are commonly used to demonstrate the quality of the solution.

One way to check the convergence of the solution is to define a convergence criterion. The convergence criterion can be that the residual has decreased to a sufficient degree. Simply, residuals are the change in the equation over an iteration [37] and the default criterion is that the residual will be reduced to 10^{-3} [35]. When the convergence criterion has been reached, the solution has converged [35][37]. However, sometimes the residual will not fall below the criterion and the solution can be considered as converged if the solution no longer changes with respect to the number of iterations [35].

Grid independence should be checked through a mesh convergence study, meaning that the mesh is checked to be good enough to not affect the solution. A mesh convergence study can be performed by starting with a coarse mesh, calculating a fluid property, e.g. drag force, followed by refining the mesh and calculating the same property again. By repeating this procedure until the fluid property has converged to a certain value, it can be assured that the mesh is good enough to not affect the solution. In order to save computational cost, a coarser mesh can be used, under the assumption that the deviations are known and that the coarser mesh provides results with acceptable accuracy.

If the quality is demonstrated with the dimensionless wall distance, the value of y^+ is checked. Depending on if a near-wall turbulence model or a wall functions is used, the value of y^+ should correspond to the limits presented in section 4.2.1.

4.9 Visualisation

The result of the simulations relevant for the resistance prediction is firstly the drag force, which in ANSYS FLUENT represents the total resistance force containing both the pressure and viscous forces. It is also of interest to check the contribution and magnitude of the pressure and viscous forces which can be done through a force report. Note that if the port-starboard symmetry is used, only half of the hull is simulated and thus, only half of the total forces are calculated.

In order to verify the quality, the residuals will be plotted and should be checked. A contour plot of the water volume fraction on the hull is also of interest in order to see if numerical ventilation has occurred.

5. Evaluation of methods

To evaluate the different methods, a set of criteria is required. The project triangle presented in figure 11 is often used to illustrate time, cost and performance as competing constraints as well as criteria to measure whether or not the project goal is met. [38]

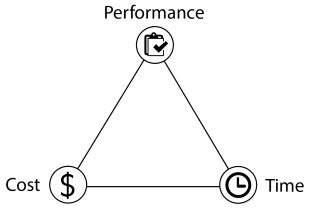

Figure 11: The project triangle.

However, there might be more competing constraints than these three when deciding which method to implement in the ship design process. For a small company like X Shore, one limitation is the accessibility of each method. A clarification of what each criterion means in this study is presented below.

Time refers to the total time consumption, including determining input values, performing calculations, and post-processing and interpreting results.

Cost is the total economical cost of applying a method. This includes the cost of software licenses, necessary tools such as high-performance computers, and the cost of work hours required to apply the method.

Performance can be scope, technology or quality [38], and is sometimes substituted by one of these in the project triangle. In this study, performance is substituted by quality and consists of the accuracy and precision of the results of each method. Accuracy refers to the deviations between results and the true value, and precision refers to the consistency of the results, i.e. that the error is consistent.

Accessibility includes the tools, facilities and competence required to apply the method as well as interpret the results. Low accessibility indicates that more tools, facilities and competence is required, compared with a method with higher accessibility.

Each method in this study will be evaluated with regard to the four criteria in figure 12. Most likely, one method will not fulfill all criteria, and choosing the most suitable method for X Shore will be a trade-off between them. It is therefore necessary to perform a systematic assessment of each method.

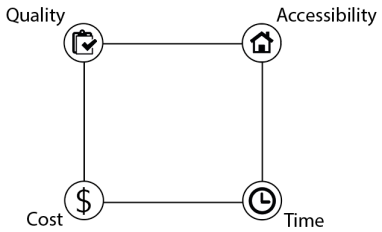

Figure 12: Evaluation criteria for this study.

5.1 Evaluation tool

Multi-criteria decision analysis (MCDA) is a tool used to assess and order a finite number of options with regard to several criteria. The tool includes a wide range of approaches with varying complexity, where most of the approaches have the performance matrix in common. In the most basic performance matrix, each row represents an alternative and each column a criterion. The criteria are weighted to indicate importance, and the options are assigned a score for each criterion, that represents how well the option meets that particular criterion. However, MCDA lacks a reference option, and consequently, the tool does not indicate if the assessed options are better than the option of doing nothing. [39]

The Pugh Matrix is a system engineering tool used to evaluate and compare design concepts [40]. It is very similar to MCDA, but has a reference that the alternatives are compared with. Since model tests already have been performed and can serve as a reference method, the Pugh Matrix is used for evaluation and the design concepts are replaced with the resistance prediction methods. The Pugh Matrix is a tool that is easy to use whenever a decision between a number of alternatives is needed and provides a simple way of taking multiple factors into account in the decision making [40].

The basic concept of the matrix can be seen in table 2, in which three methods are evaluated against four criteria. The idea of the matrix is to select one method as the baseline, which the other methods are compared against for each criteria. The baseline method will be valued as 0 for each criteria and the other methods will be compared and evaluated on a scale from -2 to $+2$ depending on if it is worse or better than the baseline method for each criteria. To get an even better differentiation and to gain more a robust assessment, the criteria are weighted from $1-5$ depending on the importance of the criteria. [40] Finally, the total score is calculated for each method by multiplying the weight with the evaluated score for each criteria respectively and summing up the calculated score for each method [40].

Table 2: Pugh Matrix.

Criteria	Weight	Baseline	Method 1	Method 2	Method 3
Criteria 1	4	0	-1	-1	+1
Criteria 2	1	0	+1	+2	-1
Criteria 3	3	0	+1	-1	+2
Criteria 4	5	0	+2	+2	-2
Score		0	7	5	-1

In a Pugh Matrix, the method ending up with the highest score is the winner. However, there is quite often not a clear winner but a clear loser when performing a Pugh Matrix and interpreting the results often includes performing a sanity check. The quality of the decision is also clearly depending on the selection of criteria and how well-defined the criteria are. [40]

6. Results

The purpose of this chapter is to present how to apply Holtrop & Mennen, the Savitsky method and a CFD-simulation. The results from applying each method on Eelex 2020 will be compared and evaluated against the criteria from chapter 5. To enable a comparison, the characteristics for Eelex 2020 identified in the conducted model tests are used as input values in the three applied methods. For the same reason, the water density ρ and kinematic viscosity ν are assumed to be the same as in the model tests, $\rho = 1026.06$ kg/m^3 and $\nu = 1.1892 \cdot 10^{-6}$ m^2/s. Furthermore, the results from the model tests are re-calculated and does not include resistance from appendages. The sections below describe how to find the input values if no model test results are available or if any of the input values are missing from the tests. The latter is the case for some of the input values used in the applied methods.

6.1 Results from previous studies

Several studies comparing resistance from CFD with experimental values have been conducted. A study from MIT that evaluated hull resistance for speeds corresponding to Froude numbers $F_n \leq 0.41$, reports that the maximum error was an over-prediction by 8.2% [7]. Another report studying two displacing hulls at Froude numbers $0.22 < F_n < 0.44$, presents a maximum error of 1.3% and 4.1% for the hulls respectively [33]. In contrast to the findings from MIT, another study shows that for planing hulls and $F_n > 1.3$, CFD under-estimates the total resistance by 8.2% [10]. Brizzolara and Serra [41] conclude that an under-estimation of 10% can be expected when CFD is applied. Furthermore, CFD is shown to be more accurate than the Savitsky method [41] and Çakıcı et al. [25] found a difference of 7.8% when comparing CFD and the Savitsky method at $F_n = 1$. Nikolopoulos and Boulougouris [17] have applied Holtrop & Mennen on 11 different hulls operating in speeds corresponding to $F_n < 0.2$. In some cases, the method over-estimates the resistance, while it under-estimates it in other cases. The maximum error is an over-prediction of 16%. However, they point out that in cases where the hull geometry is close to the applicability limits, the accuracy might decrease. In conclusion, it is common that the CFD results are within 10% of the experimental values, while the errors for the Savitsky method and Holtrop & Mennen generally are larger.

The resistance is difficult to predict for planing hulls. According to Brizzolara and Serra [41], one reason for this is that both the viscous and pressure components are related to the trim moment and the dynamic lift force in a non-linear way. Consequently, it is crucial to accurately predict trim and sinkage in order to obtain an accurate result of the total resistance. Frisk and Tegehall [10] identified difficulties when simulating free sinkage and trim in ANSYS FLUENT. Instead of finding an equilibrium position, the free surface moved with the dynamic mesh, which caused the hull to oscillate with increasing amplitude.

6.2 Holtrop & Mennen

This section presents the suggested approach to Holtrop & Mennen, followed by the results from applying the method on Eelex 2020. The suggested approach is a Python 3 program developed by the authors to calculate resistance according to Holtrop & Mennen. The program is based on equations in Appendix A and the graphical user interface is based on an open source library, graphics.py [42].

6.2.1 How to apply Holtrop & Mennen

The program starts with showing an input window and the inputs required are presented below in table 3 in the same order as they appear in the program's input window. All input values should be given in SI-units. The interface of the input window can be seen in Appendix C in figure C.1.

Table 3: Input parameters for Holtrop & Mennen.

Input	Description	Symbol	Figure reference
Afterbody form	A value reflecting the afterbody form of the hull, i.e. if it has a V-shaped, normal shaped or U-shaped afterbody the input value is 1, 2 or 3 respectively.	-	-
The transverse area of the transom	The immersed part of the transverse area of the transom at zero speed	A_T	Figure 13b
Area of immersed midship section	The immersed midship section at $L_{WL}/2$	A_M	Figure 13c
The waterplane area	The horizontal area of the hull at the waterline	A_{WP}	Figure 13d
Beam	Width of the boat at the widest point	B	-
Weight	The total weight of the boat	m	-
Length on waterline	Length at the level where it sits in the water	L_{WL}	Figure 14
Length between perpendiculars	Distance between aft and forward perpendiculars	L_{PP}	Figure 14
Draught at forward perpendicular	Measured in the perpendicular of the bow	D_{FP}	Figure 14
Draught at aft perpendicular	Measured in the perpendicular of the stern	D_{AP}	Figure 14
Longitudinal center of buoyancy	Measured from the aft	LCB	Figure 14

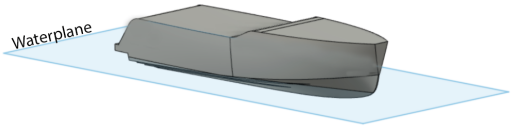

(a) The hull on the free surface.

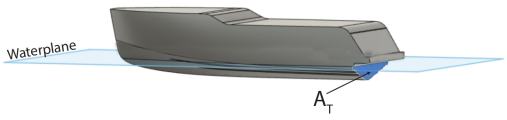

(b) The immersed part of the transverse area of the transom at zero speed.

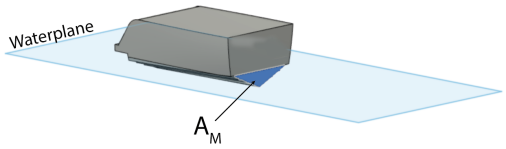

(c) The immersed midship section area.

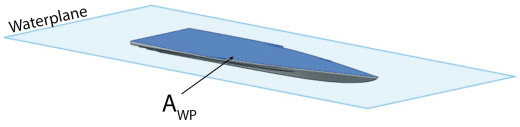

(d) The waterplane area.

Figure 13: Clarification of A_T, A_M and A_{WP}.

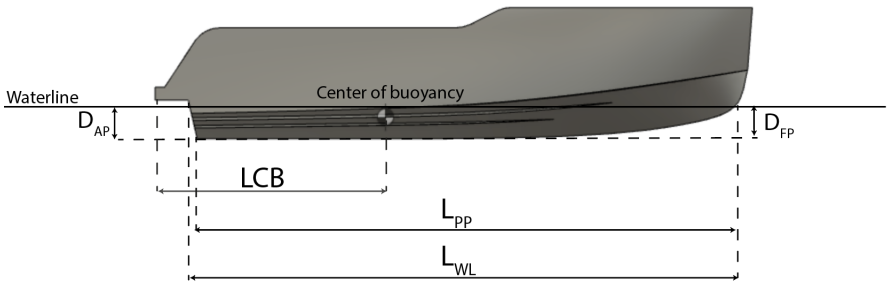

Figure 14: Figure showing L_{WL}, L_{PP}, D_{FP}, D_{AP} and LCB.

The results are then presented in a new output window, the interface can be seen in Appendix C in figure C.2. The first row presents the different speeds in knots used in the calculations. The second row shows the Froude number F_n for the different speeds, calculated according to equation 24. The Froude number indicates whether or not the vessel is displacing. The next seven rows in the table presents the resistance components in newton in the total resistance equation 17 for the Holtrop & Mennen method. The last three rows present the total resistance, first the resistance force in newton, followed by the resistance power in horsepower and watts.

6.2.2 Holtrop & Mennen applied on Eelex 2020

Table 4 presents the input values used when applying Holtrop & Mennen on Eelex 2020. The total time required to perform the method is approximately 30 minutes, where the main part is to determine the input values. When the input values are determined, the calculation time is a few seconds, and no post-processing is required.

Table 4: The input values used when applying Holtrop & Mennen on Eelex 2020.

	Symbol	**Value**	**Unit**
Afterbody form		1	
Transverse area of transom	A_T	0.447	m^2
Area of immersed midship section	A_M	0.4381	m^2
Waterplane area	A_{WP}	12.73	m^2
Beam	B	2.550	m
Length on waterline	L_{WL}	7.414	m
Length between perpendicular	L_{PP}	7.489	m
Weight	m	2600	kg
Draught at forward perpendicular	D_{FP}	0.417	m
Draught at aft perpendicular	D_{AP}	0.382	m
Longitudinal position of the center of buoyancy	LCB	2.664	m

The results are shown in table 5.

Table 5: The resulting values when applying Holtrop & Mennen on Eelex 2020.

		4 knots	**5 knots**	**6 knots**	**7 knots**	**8 knots**
Froude number	F_n	0.24	0.3	0.36	0.42	0.48
Frictional resistance	R_F	71.4 N	107.5 N	150.2 N	199.3 N	254.8 N
Form factor	$1 + k_1$	2.2	2.2	2.2	2.2	2.2
Resistance of appendages	R_{APP}	0 N	0 N	0 N	0 N	0 N
Wave-making and wave-breaking resistance	R_W	41.2 N	265.6 N	1002.1 N	1509.0 N	1984.3 N
Resistance due to bulbous bow near the surface	R_B	0 N	0 N	0 N	0 N	0 N
Resistance of immersed transom stern	R_{TR}	138.5 N	194.6 N	248.8 N	296.0 N	330.8 N
Model-ship resistance	R_A	19.6 N	30.7 N	44.2 N	60.1 N	78.6 N
Total resistance	R_{total}	358 N	729 N	1628 N	2308 N	2960 N
Total resistance power	R_W	736 W	1877 W	5027 W	8311 W	12181 W
Total resistance power	R_{hp}	1 hp	2 hp	6 hp	11 hp	16 hp

The contribution to the total resistance from the resistance components in the Holtrop & Mennen method are illustrated in figure 15. The method is applied for the speed range $2-8$ knots and it can be seen that the greatest impact on the total resistance as the speed increases is the wave-making and wave-breaking resistance.

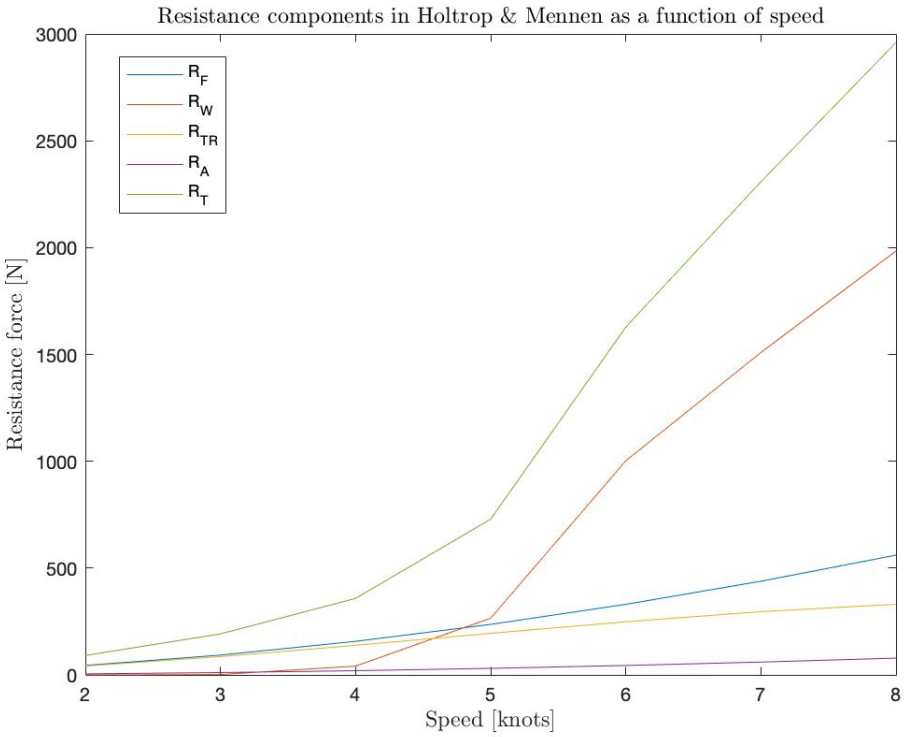

Figure 15: The contribution of the resistance components in Holtrop & Mennen.

The applicability criteria for Holtrop & Mennen, presented in section 3.1, are checked for each speed. As can be seen in table 6, the length-beam ratio criteria is not fulfilled for any of the speeds and the Froude number criteria is not fulfilled for the speed of 8 knots. However, the prismatic coefficient is met for all the displacement speeds.

Table 6: Criteria for Holtrop & Mennen applicability.

	Froude number	Prismatic coefficient	Length-beam ratio
	$F_n < 0.45$	$0.55 \leq C_P \leq 0.85$	$3.9 \leq L_{WL}/B \leq 9.5$
4 knots	0.24	0.77	2.9
5 knots	0.30	0.77	2.9
6 knots	0.36	0.77	2.9
7 knots	0.42	0.77	2.9
8 knots	0.48	0.77	2.9

If any of the criteria are not met, the results for that speed will be printed in red in the output window of the developed program.

6.3 Savitsky

This section presents the suggested approach to the Savitsky method, followed by the results from applying the method on Eelex 2020. The suggested approach is a Python 3 program developed by the authors to calculate resistance according to Savitsky. The program is based on equations in Appendix B and the graphical user interface is based on an open source library, graphics.py [42]. The specific weight of water φ is assumed to be 9.789 kN/m^3.

6.3.1 How to apply the Savitsky method

The program starts with showing an input window and the inputs required are presented below in table 7 in the same order as they appear in the program's input window. All input values should be given in meter, kilogram or degrees. The interface of the input window can be seen in Appendix D in figure D.1.

Table 7: Input parameters in the Savitsky method.

Input	Description	Symbol	Figure reference
Displacement	Total weight of the boat	Δ	-
Length between perpendiculars	Distance between aft and forward perpendiculars	L_{PP}	Figure 14
Longitudinal centre of gravity	Distance from stern to the centre of gravity, measured along the keel	LCG	Figure 16a
Vertical centre of gravity	Distance from keel to the centre of gravity, measured normal to the keel	VCG	Figure 16a
Beam	Width of the boat at the widest point	B	Figure 16b
Deadrise angle	Angle of the v-shape at the stern, measured from horizontal plane to bottom of the boat	β	Figure 16b
Angle between keel and propeller shaft	Inclination of the thrust line relative to the keel	ϵ	Figure 16a
Distance between propeller shaft and centre of gravity	Measured normal to the extension of the shaft line	f	Figure 16a

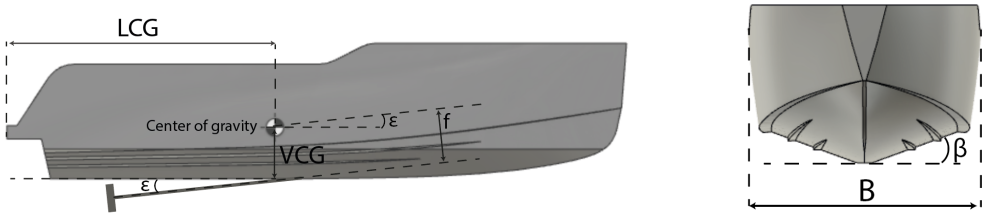

(a) Figure showing LCG, VCG, ϵ and f.

(b) Figure showing B and β.

Figure 16: Clarification on input values for the Savitsky method.

The results are then presented in a new window, see figure D.2 in Appendix D. The first row presents the different speeds in knots used in the calculations. The second row shows the Froude

number F_n for the different speeds, calculated according to equation 24. The Froude number indicates whether or not the vessel is fully planing. The third row in the table presents the equilibrium trim angle, i.e. the angle the boat will have when going in constant speed, and the fourth row presents the draught at the transom. The last three rows present the total resistance, first the resistance force in newton, followed by the resistance power in watts and horsepower.

6.3.2 The Savitsky method applied on Eelex 2020

Table 8 presents the input values when applying the Savitsky method on Eelex 2020. The total time required to perform the method is approximately 30 minutes, where the main part is to determine the input values. When the input values are determined, the calculation time is a few seconds, and no post-processing is required.

Table 8: The input values when applying the Savitsky method on Eelex 2020.

	Symbol	**Value**	**Unit**
Displacement	Δ	2600	kg
Length between perpendiculars	L_{PP}	7.498	m
Longitudinal centre of gravity	LCG	3.081	m
Vertical centre of gravity	VCG	0.718	m
Beam	B	2.550	m
Deadrise angle	β	15	deg
Angle between keel and propeller shaft	ϵ	6	deg
Distance between propeller shaft and COG	f	0.6	m

The input in table 8 resulted in the values presented in table 9.

Table 9: The resulting values when applying the Savitsky method on Eelex 2020.

		12 knots	**16 knots**	**20 knots**	**24 knots**	**32 knots**
Froude number	F_n	0.72	0.96	1.20	1.44	1.92
Equilibrium trim	τ	3.97°	4.27°	3.81°	3.23°	2.37°
Resistance force	R_{total}	2604 N	3114 N	3379 N	3690 N	4641 N
Resistance power	R_W	16.1 kW	25.6 kW	34.8 kW	45.5 kW	76.4 kW
Resistance power	R_{hp}	21.5 hp	34.4 hp	46.6 hp	61.1 hp	102.4 hp

The applicability criteria for the Savitsky method, presented in section 3.2, are checked for each planing speed, table 10.

Table 10: Criteria for Savitsky applicability.

	Speed coefficient $0.6 \leq C_V \leq 13$	Trim angle $2° \leq \tau \leq 15°$	Wetted length-beam ratio $\Lambda \leq 4$
12 knots	1.23	3.97°	2.5
16 knots	1.65	4.27°	2.07
20 knots	2.06	3.81°	1.87
24 knots	2.47	3.23°	1.77
32 knots	3.29	2.37°	1.63

As can be seen in the table 10, all the criteria are fulfilled for each speed which indicates that the method should be applicable on Eelex 2020. If any of the criteria are not met, the results for that speed will be printed in red in the output window of the developed program.

After further investigation, it was found that the applicability criteria for the Savitsky method is met even for the speeds 7 and 8 knots even though they are not planing speeds. The results from applying the Savitsky method for 7 and 8 knots can be seen in table 11.

Table 11: The resulting values when applying the Savitsky method on Eelex 2020 for 7 and 8 knots.

		7 knots	**8 knots**
Froude number	F_n	0.42	0.48
Equilibrium trim	τ	2.88°	3.04°
Resistance force	R_{total}	1657 N	1823 N
Resistance power	R_W	5966 kW	7500 kW
Resistance power	R_{hp}	8.0 hp	10.1 hp

6.4 CFD

This section presents how the CFD simulation on Eelex 2020 was conducted. The presented setup is the suggested approach for how to do the simulations and they are performed in ANSYS FLUENT 19.0. A step-by-step tutorial on how to perform the simulations has been made and was given to X Shore.

6.4.1 Assumptions and limitations

To start with, the fluids air and water are assumed to be incompressible resulting in that velocity and pressure fields are independent from the temperature field. The approach is based on the theory presented in chapter 4 and it should be noted that the ITTC guidelines [23] are intended for applications with high Reynolds numbers and Froude numbers of the order of 0.1 and rarely above 1. These conditions are fulfilled for Eelex 2020 in displacement speeds, but when reaching top speeds, the guidelines have not been proven valid.

Several attempts of dynamic meshing were made, but problems with negative cell volume occurred. The problem can probably be fixed by reducing the time step and/or refining the mesh. However, due to time and hardware limitations, it was decided to focus on static simulations. Therefore, the following results are obtained from static simulations and no dynamic mesh have been used. Consequently, the simulations do not capture hull motion, such as heave and pitch,

and the running attitude is hence not identified by the simulations themselves. To capture the impact of the running attitude, the draught and trim were needed to be manually implemented in the static setup. The discovered hardware limitations pointed out the importance of sufficient hardware performance in this type of simulations. Initially, an attempt to perform both dynamic and static simulations was made on a computer with 16 GB RAM and a 1.33 GHz processor with 8 cores. The attempts were unsuccessful due to lack of RAM, which resulted in both mesh limitations and extremely high computational time. Therefore, the computer used in this project has 64 GB RAM and a 3.6 GHz processor with 8 cores, which was sufficient for the static simulations.

6.4.2 Geometry and computational domain

The geometry of Eelex 2020 was imported as a CAD-file in STEP format, since it is a compatible file format with ANSYS FLUENT. The port-starboard symmetry was used, and only half of the hull was simulated. The computational domain was built as a rectangular block around the hull, with the smallest dimensions possible according to the ITTC guidelines in order to reduce the number of cells. The coordinate system was located at the symmetry plane, 38 mm below the free surface at zero speed and 465 mm forward the aft of the the hull. Ideally, the coordinate system should be placed at the draught at zero speed in order to simplify the setup. Measured from the coordinate system, the inlet and outlet were placed approximately $2L_{PP}$ and $3L_{PP}$ forward and backward, respectively, and the other boundaries were placed approximately $1L_{PP}$ away. In order to enable for refinements around the free surface, a smaller rectangular block was built around the free surface area. This rectangular block had the same length and width as the whole computational domain, but the height was set to 0.25 m upwards and 0.5 m downwards measured from the coordinate system. Before proceeding, the imported hull surface was subtracted from the domain. The computational domain and the associated dimensions can be seen in figure 17 and table 12.

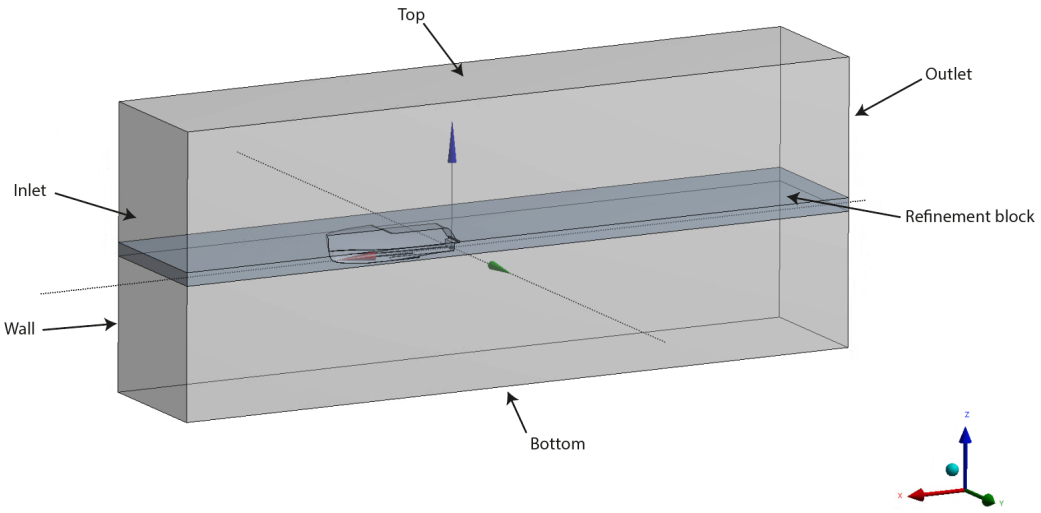

Figure 17: The computational domain.

Table 12: The dimensions of the computational domain measured from origo.

	Inlet	**Outlet**	**Top**	**Bottom**	**Wall**
Computational domain	16 m	−24 m	8 m	−8 m	8 m
Refinement block	16 m	−24 m	0.25 m	−0.5 m	8 m

6.4.3 Mesh

The domain was meshed using the function body of influence in order to achieve the refinements around the surface. To capture the boundary layer, an automatic prism layer with 15 layers was added to the hull with a first layer thickness of $2.7 \cdot 10^{-4}$ m and a growth rate of 1.2. This corresponds to a dimensionless wall distance $y^+ = 30$ for 7 knots and was set in order to prevent numerical ventilation. The prism layer in the aft of the hull can be seen in figure 18. For the hull surface, the function face sizing was used and the element size was set to 0.1 m. The final mesh was chosen based on the grid dependence study, see section 6.4.5.

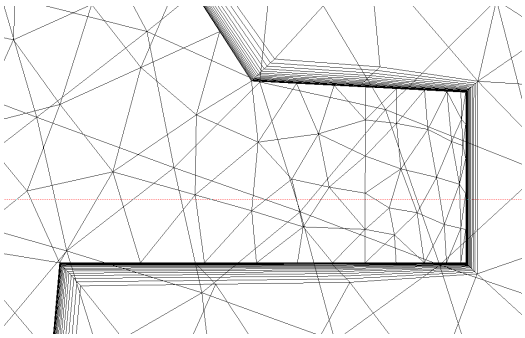

Figure 18: The prism layer in the aft of the hull.

6.4.4 Model setup

In the model setup, the mesh was converted to polyhedral cells. The two models applied to the simulations was the viscous model and multiphase model. For the viscous model, the SST k-ω model was chosen and for the multiphase, the VOF was used as model, open channel flow as VOF sub-model, implicit as volume fraction formulation and the body force formulation was set as an implicit body force. The material for the two phases in the multiphase was defined as air and water. For water, the density and viscosity were changed to 1026.06 kg/m^3 and 0.0012 kg/ms respectively. The gravity force was defined as 9.81 m/s^2 in negative z-direction. To satisfy the time step criterion for the SST k-ω turbulence model, the time step was calculated according to equation 31 and resulting values used in the simulations are presented in table 13. The number of iterations was set to 1000 for all the performed simulations.

Table 13: The time steps used in the simulations.

	Time step		**Time step**
4 knots	0.03	**12 knots**	0.011
5 knots	0.02	**16 knots**	0.009
6 knots	0.02	**20 knots**	0.007
7 knots	0.02	**24 knots**	0.006
8 knots	0.015	**32 knots**	0.004

The boundary condition for the inlet was set as an pressure inlet, due to the fact that the open channel flow model is used. The outlet was set to a pressure outlet, the hull, top and bottom were set to wall and the symmetry plane to symmetry. For the in- and outlet the turbulence intensity and the turbulent viscosity ratio was set to default, i.e. 5 % and 10, respectively. The free surface was varying with the speed and the bottom level was set to -8 m.

Since the VOF model is applied, the pressure-based solver is used and the solution is set to be steady state. The solution method used is a coupled scheme and the second-order upwind scheme

is chosen for all but the gradient, the pressure and volume fraction discretizations were least square cell based, PRESTO! and compressive is used, respectively. The quality of the simulations was ensured by a residual criteria of 10^{-3} and a mesh convergence study.

6.4.5 Mesh convergence

A mesh convergence study was made in order to ensure the quality of the results. The study was performed on four different meshes for the Froude number $F_n = 0.42$, corresponding to 7 knots. The number of cells, cell size at the free surface, if the solution converged or not and the resulting total resistance coefficient C_T can be seen in table 14, for each mesh.

Table 14: Grid dependence study of Eelex 2020 for $F_n = 0.42$.

Mesh number	Number of cells	Cell size at free surface	Converged	C_T
1	4218791	0.095 m	No	-
2	5563201	0.085 m	Yes	$10.5 \cdot 10^{-3}$
3	7750496	0.075 m	Yes	$10.6 \cdot 10^{-3}$
4	88799451	0.03 m	Yes	$10.5 \cdot 10^{-3}$

As can be seen in table 14, a refinement of the mesh from 5.56 million to 88.8 million cells does not affect the total resistance coefficient. However, an even coarser mesh, mesh number 1 with 4.2 million cells, results in a solution that does not converge. The mesh used in the simulations is mesh number 2, since a finer mesh will contribute to higher computational cost without increasing the accuracy. With mesh number 2, simulating one speed, including setting up the computational domain, running the calculations and interpreting the results, can be done within one day. The entire speed range can be simulated in approximately one week, excluding the mesh convergence study. The height of the cells at the free surface should ideally be 0.01% of the hull's length of the waterline. However, that resulted in a mesh size beyond the computer's capacity, so the cell size needed to be adjusted. For mesh number 2, the cell size at the free surface is 0.085 m, which corresponds to 1.1% of the waterline length. However, the mesh convergence study shows that refining the mesh at the free surface to 0.04% of the waterline length, as in mesh number 4, does not affect the accuracy. In summary, mesh number 2 is assumed to give sufficient accuracy, and can be seen in figure 19.

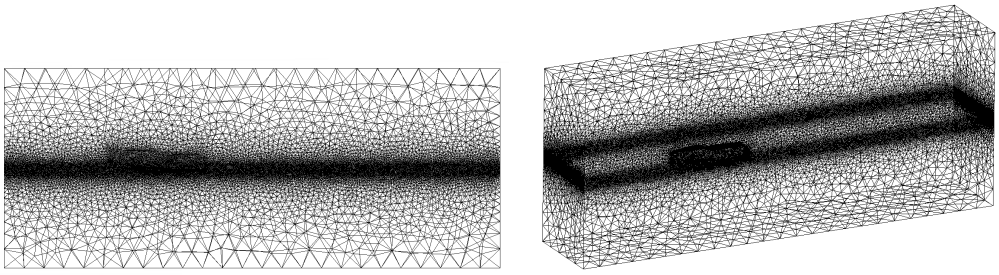

(a) The mesh from the symmetry plane. (b) Overview of the mesh.

Figure 19: The 5.56 million mesh.

Note that the mesh is not hollow, the mesh in figure 19b is only showing mesh on the outer edges of the computational domain.

6.4.6 Results from the CFD simulations

The CFD simulations on Eelex 2020 has been performed for the whole speed range, i.e. for $4 - 32$ knots, with two different setups regarding the location of the free surface. Both setups are simu-

lated without trim, because the identified method to change the trim angle requires modifications in the CAD-model and remeshing of the computational domain. This procedure is time consuming and due to time limitations the simulations were initially performed without any trim angle. Consequently, this will affect the accuracy of the results for the higher speeds.

The location of the free surface is referred to as ΔWL, which is the change of waterline length, where $\Delta WL = 1$ is the waterline length at zero speed. It is assumed that the change in waterline length is proportional to the change in draught, e.g. $\Delta WL = 0.9$ corresponds to 90% of the waterline, and 90% of the draught at zero speed. The first setup is presented in table 15 where the free surface in located at the draught at zero speed for all speeds up to 12 knots, $\Delta WL = 1$. For the higher speeds, a lift force is assumed to be acting on the hull and therefore the free surface is assumed to be lower, $\Delta WL = 0.9$. The differences in total resistance compared to the model tests results are presented as *Diff. in res.* in table 15.

Table 15: The resulting resistance in when applying CFD on Eelex 2020 with setup 1.

	Total resistance	ΔWL	Diff. in res.
4 knots	390 N	1	11.43%
5 knots	542 N	1	−11.58%
6 knots	822 N	1	−13.84%
7 knots	1014 N	1	−32.26%
8 knots	1284 N	1	−43.39%
12 knots	2596 N	1	−21.09%
16 knots	3268 N	0.9	−14.7%
20 knots	4666 N	0.9	19.15%
24 knots	6254 N	0.9	45.87%
32 knots	10156 N	0.9	77%

In order to investigate the importance of the location of the free surface level, the second setup uses the ΔWL from the model tests to place the free surface level. The used values of ΔWL, as well as the total resistance compared to the model tests results for the second setup can be seen in table 16.

Table 16: The resulting resistance in when applying CFD on Eelex 2020 with setup 2.

	Total resistance	ΔWL	Diff. in res.
4 knots	390 N	1	11.43%
5 knots	542 N	1	−11.58%
6 knots	822 N	1	−13.84%
7 knots	1008 N	0.99	−32.67%
8 knots	1134 N	0.96	−49.21%
12 knots	1832 N	0.86	−44.32%
16 knots	2192 N	0.74	−42.78%
20 knots	3144 N	0.72	−19.71%
24 knots	4362 N	0.72	1.77%
32 knots	8046 N	0.76	40.84%

It can be seen in table 15 and 16 that the location of the free surface have a great impact on the results, especially for the planing speeds, which was expected due to the impact of the running attitude. For semi-planing speeds, a more accurate location of the free surface results in less accurate resistance predictions, which might be explained by the lack of trim angle. In order to get the most accurate resistance predictions, it has been decided to proceed with the results from setup 1 for speeds up to 16 knots and the results from setup 2 for higher speeds.

The pressure resistance, viscous resistance and total resistance forces are presented in table 17

Table 17: The resulting resistance when applying CFD on Eelex 2020.

	4 knots	**5 knots**	**6 knots**	**7 knots**	**8 knots**
Pressure resistance	320 N	436 N	690 N	840 N	1018 N
Viscous resistance	70 N	106 N	132 N	174 N	266 N
Total resistance	390 N	542 N	822 N	1014 N	1284 N
	12 knots	**16 knots**	**20 knots**	**24 knots**	**32 knots**
Pressure resistance	1950 N	2222 N	1980 N	2680 N	4860 N
Viscous resistance	646 N	1044 N	1164 N	1682 N	3186 N
Total resistance	2596 N	3268 N	3144 N	4362 N	8046 N

According to the theory in section 2.1, the viscous resistance should be dominating in the displacement speeds. However, it can be seen in table 17 that the pressure resistance is larger than the viscous resistance for all speeds in the CFD simulations. Figure 20 shows the volume fraction on the bottom of the hull, i.e. the distribution of the two phases air and water occupying the hull surface for all different speeds. Water is displayed in red and air in blue.

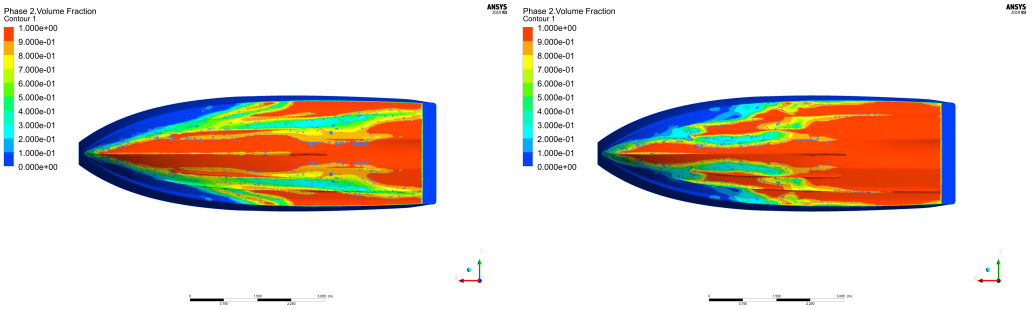

(a) 4 knots.

(b) 5 knots.

(c) 6 knots.

(d) 7 knots.

(e) 8 knots.

(f) 12 knots.

(g) 16 knots.

(h) 20 knots.

(i) 24 knots.

(j) 32 knots.

Figure 20: Volume fraction on the bottom of the hull for all speeds.

6.5 Comparison

This section will present a comparison between the results from applied methods and the values from the conducted model tests. The model test results will serve as a reference value to determine the accuracy of the other methods. For displacement, the speeds $4 - 8$ knots are regarded and the model tests are compared with results from Holtrop & Mennen and CFD simulations, as well as the Savitsky method for the higher speeds in the range. For planing, the speeds $12 - 32$ knots are regarded and model tests are compared with the Savitsky method and CFD simulation results. More detailed information about the results can be found in Appendix E.

6.5.1 Resistance predictions

The resulting resistance force from all the applied methods can be seen in figure 21. Since Holtrop & Mennen is a method for displacement hulls and Savitsky is a method for planing hulls, theoretically, the semi-empirical methods should leave a gap where the resistance can not be predicted. This gap refers to the Froude numbers which characterize a semi-planing hull, which neither of the semi-empirical methods are valid for. However, since the Savitsky method is applicable from 7 knots for Eelex 2020, the semi-planing speed range is covered by the semi-empirical methods.

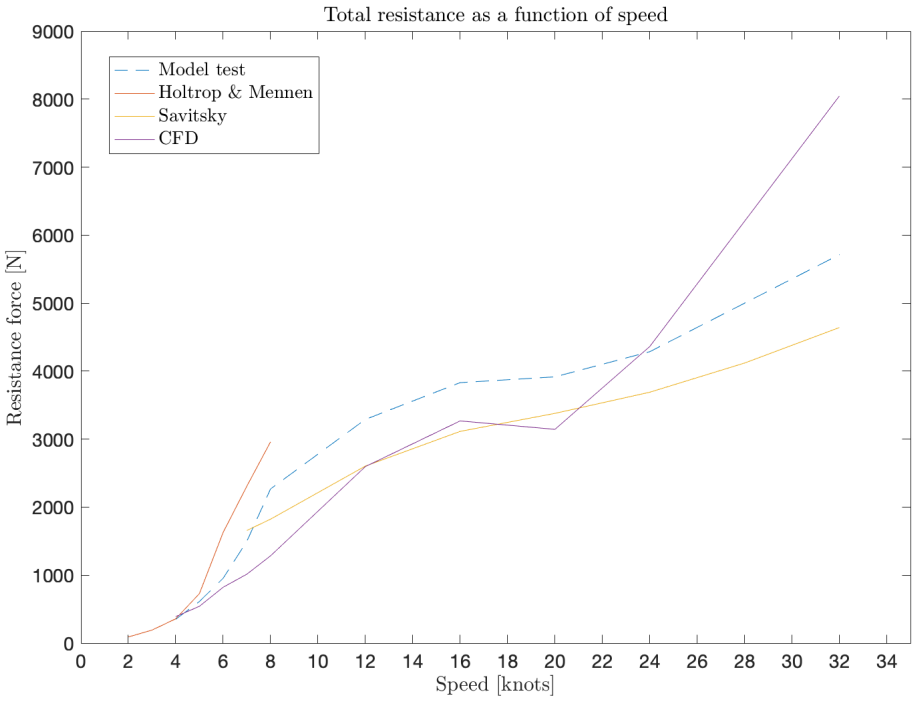

Figure 21: The resulting resistance force from all the applied methods on Eelex 2020.

For displacement speeds, i.e. the speeds $4 - 8$ knots the resulting resistance force for Eelex 2020 can be seen in figure 22.

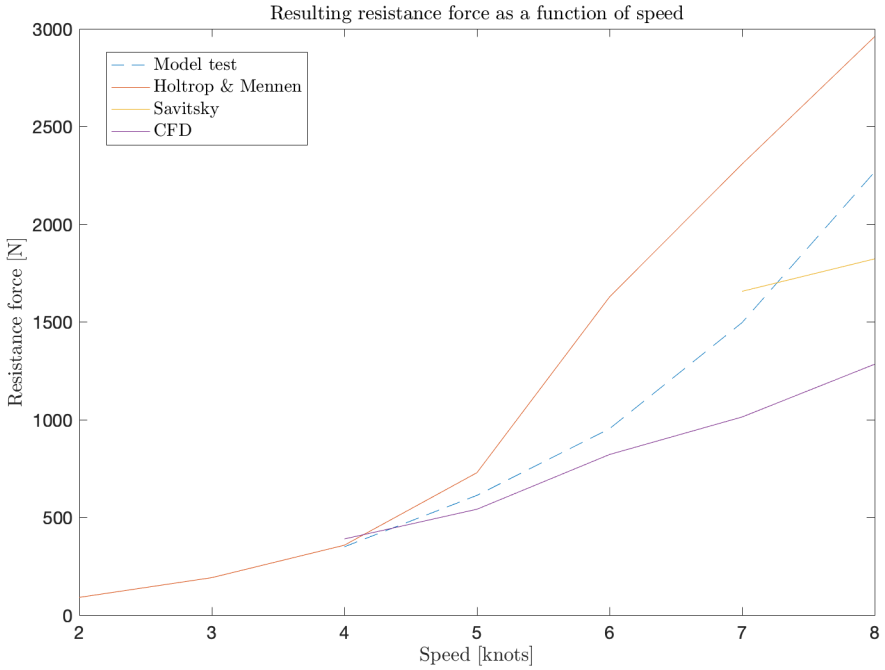

Figure 22: Resulting resistance force for Eelex 2020 in displacement speeds.

It can be seen in figure 22 that Holtrop & Mennen over-estimates the resistance, while CFD under-estimates the resistance for all speeds except for 4 knots. The difference in resistance force in percentage between Holtrop & Mennen and model test and CFD and model tests, respectively, indicates how well the methods predicts resistance assuming that the model tests provide an accurate prediction, see table 18. The difference in resistance force between the Savitsky method and model tests for 7 and 8 knots can also be seen in the table.

Table 18: Deviation in resistance force for Holtrop & Mennen, CFD and the Savitsky method from model test results.

	4 knots	**5 knots**	**6 knots**	**7 knots**	**8 knots**
Froude number	0.24	0.30	0.36	0.42	0.48
Holtrop & Mennen	2.2%	18.9%	70.6%	54.2%	30.5%
CFD	11.43%	−11.58%	−13.84%	−32.6%	−43.39%
Savitsky	-	-	-	10.7%	−19.6%

The greatest deviation for Holtrop & Mennen, 70.6%, is found Froude number $F_n = 0.36$. It is a much larger deviation than the errors found in previous studies, where a maximum of 16% was found, however for $F_n < 0.2$. For the same Froude number, $F_n = 0.36$, the deviation for CFD is -13.84% and significantly lower than the deviation for Holtrop & Mennen. The greatest deviation for CFD is found for $F_n = 0.48$ and is -43.39%. For the lower speeds in the range, the deviations are close to the 10% that are found in previous studies. Although the error increases with the speed, CFD seems to result in more accurate predictions in general. However, the Savitsky method provides results with better accuracy than both Holtrop & Mennen and CFD for 7 and 8 knots.

For planing speeds, i.e. $12 - 32$ knots, the resulting resistance force for Eelex 2020 can be seen in figure 23.

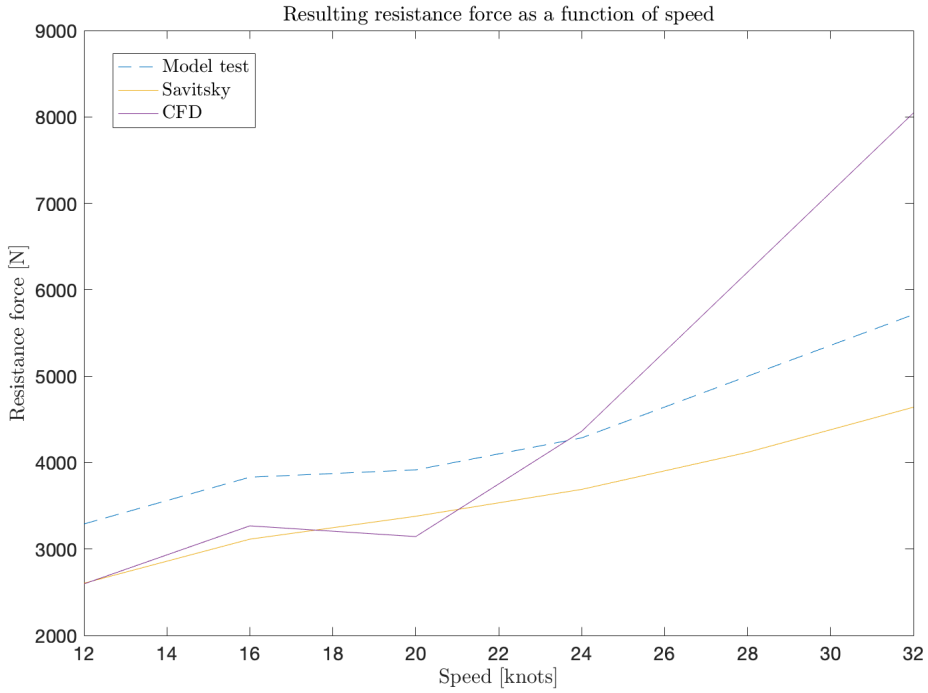

Figure 23: Resulting resistance force for Eelex 2020 in planing speeds.

In figure 23 it can be seen that CFD under-estimates the results for the lower speeds in the range, while it for the higher speeds over-estimates the resistance force. The Savitsky method is consistently under-estimating the resistance and the curves for the Savitsky method and model tests have similar shapes. The difference in resistance force in percentage between the Savitsky method and model tests, and CFD and model tests respectively can be seen in table 19.

Table 19: Difference in resistance force in percentage between model tests and Savitsky.

	12 knots	**16 knots**	**20 knots**	**24 knots**	**32 knots**
Froude number	0.72	0.96	1.20	1.44	1.92
Savitsky	-20.8%	-18.7%	-13.7%	-13.9%	-18.8%
CFD	-21.09%	-14.7%	-19.71%	1.77%	40.84%

For the Savitsky method, the largest deviation of -20.8% is found for $F_n = 0.72$. This is a significant smaller deviation than the ones found for Holtrop & Mennen at displacement speeds. The CFD results are less consistent than the results from the Savitsky method, which has an average error of 17.18%.

The Savitsky method shows good agreement on the resulting trim angles for the model tests, see figure 24, for the speeds $12 - 32$ knots. The greatest deviation of -15.3% are found for 16 knots and the smallest deviation of -4.8% for 12 knots.

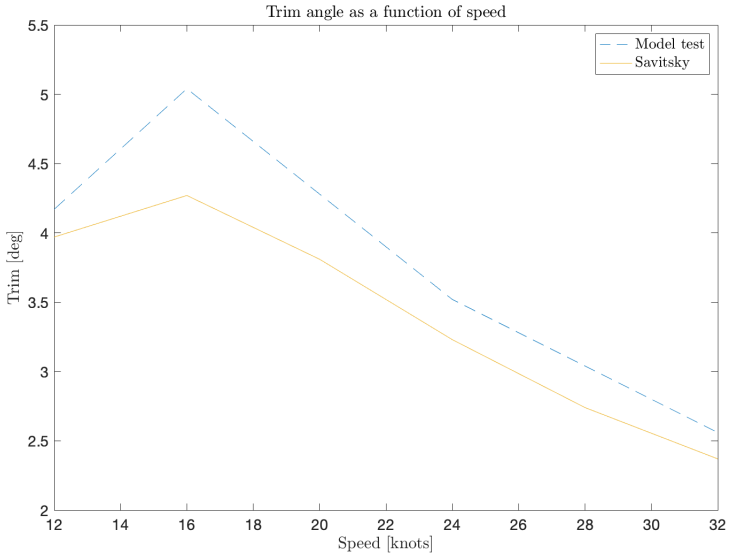

Figure 24: The resulting trim angle from model tests and the Savitsky method.

It can also be noted that Savitsky seems to under-predict the trim for the speeds $12 - 32$ knots.

6.5.2 Power predictions and efficiency

The resulting resistance power for displacement and planing speeds can be seen in table 20 and 21 respectively.

Table 20: Resulting resistance power from applying model tests, Holtrop & Mennen, CFD and the Savitsky method on Eelex 2020 in displacement speeds.

	4 knots	**5 knots**	**6 knots**	**7 knots**	**8 knots**
Froude number	0.24	0.30	0.36	0.42	0.48
Model tests	0.7 kW	1.6 kW	2.9 kW	5.4 kW	9.3 kW
Holtrop & Mennen	0.74 kW	1.88 kW	5.03 kW	8.31 kW	12.18 kW
CFD	0.80 kW	1.39 kW	2.54 kW	3.65 kW	5.28 kW
Savitsky	-	-	-	5.56 kW	7.5 kW

Table 21: Resulting resistance power from applying model tests, the Savitsky method, and CFD on Eelex 2020 in semi-planing and planing speeds.

	12 knots	**16 knots**	**20 knots**	**24 knots**	**32 knots**
Froude number	0.72	0.96	1.20	1.44	1.92
Model tests	20.3 kW	31.5 kW	40.3 kW	52.9 kW	94.0 kW
Savitsky	16.1 kW	25.6 kW	34.8 kW	45.5 kW	76.4 kW
CFD	16.03 kW	26.90 kW	32.35 kW	53.86 kW	132.46 kW

Table 22 presents the different components of the total efficiency. The first four rows represent the input values required to calculate the propulsion efficiency η_D, where the open water propeller efficiency is an estimation for the single propeller used for Eelex 2020. The last three rows present the gear box efficiency, motor efficiency and battery capacity for Eelex 2020.

Table 22: Efficiency for Eelex 2020.

	Symbol	**Value**	**Unit**
Number of propellers		1	-
Open water propeller efficiency	η_O	60	%
Relative rotary efficiency	η_R	100	%
Hull efficiency	η_H	106	%
Propulsion efficiency	η_D	63	%
Gear box efficiency	η_G	96	%
Motor efficiency	η_M	95	%
Battery capacity	E_B	120	kWh

The resulting range for Eelex 2020 from the different methods, assuming constant speed and including a sea margin of 15% to capture the influence of waves and wind, can be seen in figure 25.

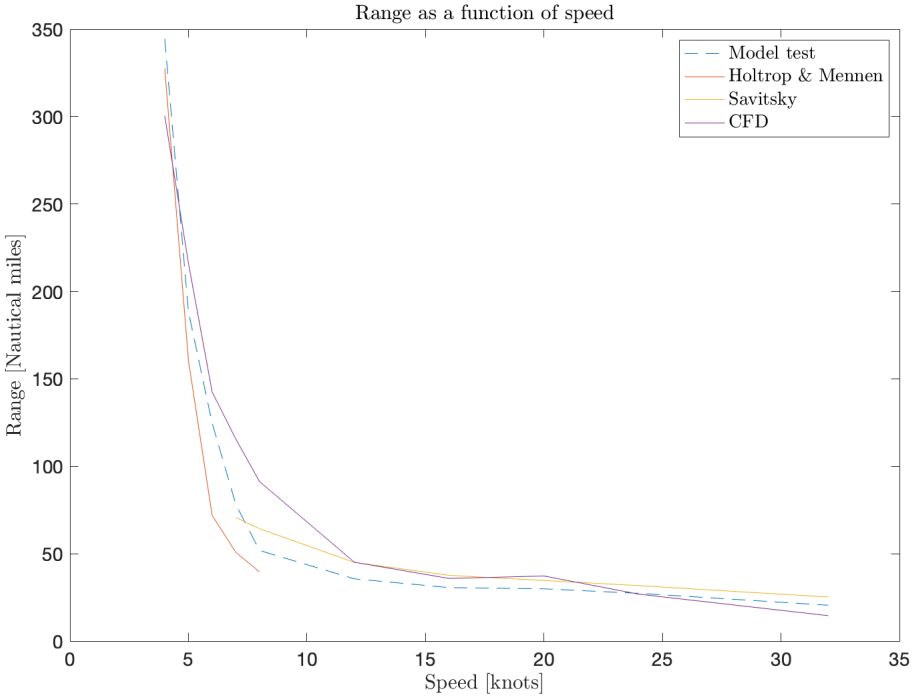

Figure 25: Resulting range for the different methods.

It can be seen in figure 25 that the range decreases significantly from approximately $300 - 50$ nautical miles (NM) for increasing speeds in the range of $4 - 12$ knots, and both Holtrop & Mennen and CFD show this behaviour. After 12 knots, the curve flattens out, and the decrease in range is not as steep as for the lower speeds, according to all methods applied in the planing speed range. The corresponding time for each range is presented in table 23 and 24.

Table 23: Resulting time and range for displacement speeds.

	Model test		**Holtrop & Mennen**		**CFD**		**Savitsky**	
	Time	Range	Time	Range	Time	Range	Time	Range
4 knots	86h	344 NM	81h	327 NM	75h	300 NM	-	-
5 knots	37h	188 NM	32h	160 NM	43h	216 NM	-	-
6 knots	20h	124 NM	12h	72 NM	23h	142 NM	-	-
7 knots	11h	78 NM	7h	50 NM	16h	115 NM	10 h	70 NM
8 knots	6h	51 NM	5h	39 NM	11h	91 NM	8 h	64 NM

Table 24: Resulting time and range for planing speeds.

	Model test		**Savitsky**		**CFD**	
	Time	Range	Time	Range	Time	Range
12 knots	3h	35 NM	3h 45 min	45 NM	3h 45min	45 NM
16 knots	1h 50min	30 NM	2h 20min	37 NM	2h 15min	35 NM
20 knots	1h 30min	29 NM	1h 45min	34 NM	1h 50min	37 NM
24 knots	1h	27 NM	1h 20min	31 NM	1h	26 NM
32 knots	40min	20 NM	45min	25 NM	30min	14 NM

It can be seen in table 24 that all of the three methods for resistance predictions in planing speeds, and especially in the cruising speed of 24 knots, give similar predictions of the range. However, for the displacement speeds the results of the range predictions are more varying.

6.6 Evaluation

Table 25 presents the evaluation of the methods in a Pugh Matrix. Model tests are set as a baseline, and each method is rated from -2 to +2 on each criterion, where -2 means that the method performs worse than the baseline on that particular criterion, and +2 better than the baseline.

The weights are relative values, where the most important criterion is assigned the highest value of the weighting scale, i.e. 5, and the least important criterion is assigned the lowest value, i.e. 1. Since the weights are not absolute values, the weighting must be re-evaluated if new criteria are added and the ranking changes. A criterion with the weight 1, is therefore not irrelevant but of less importance than criteria with a higher value.

Table 25: Pugh Matrix with X Shore's criteria.

	Criteria	Weight	**Model tests**	**Holtrop & Mennen**	**Savitsky**	**CFD**
Low time consumption	Preparing calculations	4	0	+2	+2	+1
	Performing calculations	3	0	+2	+2	-1
	Interpreting results	5	0	+2	+2	+2
Low cost	Equipment*	2	0	+2	+2	+1
High quality	Accuracy	1	0	-2	-1	-1
	Precision	3	0	-2	0	-1
High accessibility	Equipment*	5	0	+2	+2	+1
	Competence	4	0	+2	+2	0
	Score		**0**	**38**	**45**	**14**

* Equipment refers to software licenses, hardware, tools and facilities.

The method with the highest total score of 45 is the Savitsky method. Holtrop & Mennen has a slightly lower score, 38, due to its low scores on the quality criteria. CFD has the lowest total score, 14, since it is much more time consuming and has a lower accessibility than the semi-empirical methods. It can be seen in the Pugh Matrix, table 25, that low time consumption and cost, and high accessibility have higher priority than high accuracy, when choosing a method to predict resistance in the design phase. Accuracy is therefore assigned the weight 1, not because it is irrelevant, but because it has lower priority. However, precision which is the other quality criteria is weighted higher since the consistency of the results determines if the method can be used at all.

A low time consumption is of high importance, due to the fast-paced design processes at the company. It can be seen in the matrix that it is more important that determining input values and interpreting results are less time consuming than the importance of the time spent on performing the calculations. This means that the most important aspect of low time consumption is the active work hours spent on the task. If running a CFD-simulation takes hours, or days, without demanding active work hours and deliver results within time plan, it can still be a suitable method. The cost of equipment is ranked lower than both time consumption and accessibility. While cost is an important aspect, equipment cost is assumed to be spread out over a long period of time. It might therefore be less expensive to invest in equipment to enable in-house approaches than to constantly hire external consultants. Cost will consequently have less importance and not be a deciding factor. The accessibility of the equipment is however of bigger importance in order to enable in-house approaches. The same goes for competence, since competence deficiencies in the company require external consultants. Note that the weighting is set based on the purpose of this study, i.e. to find a suitable approach to predict resistance for X Shore as a start-up company.

7. Discussion and Conclusion

All resistance predictions are made on a bare hull and in calm water conditions. When converting the resistance to range, a sea margin has been included in order to increase the accuracy of the range estimations. However, the estimated ranges for different speeds are, despite the sea margin, higher than the ranges that can be expected from a real life scenario, where resistance from appendages are present. Adding resistance from appendages will give more accurate results, but requires modifications of the methods investigated in this study. Several aspects considering the efficiency might influence the outcomes of the methods, e.g. the hull efficiency which is calculated using simplified equations and the open water propeller efficiency which is assumed to be constant over the entire speed range. Moreover, energy losses from the batteries to the motor are not accounted for. Since the study is limited to one hull, no conclusions can be drawn about the performance of the methods in general.

The quality of the outcome of the Pugh Matrix depends on the selection of criteria. In order for the Pugh Matrix to guide the decision making process, all relevant criteria must be included, and no irrelevant criteria should be present in the matrix. The criteria in this study was selected after discussions between the authors and X Shore, and are assumed to be sufficient for the purpose of this study. However, to use this evaluation method in the future, X Shore needs to ensure that all relevant aspects are covered in the selected criteria. The company might prioritize the criteria differently in future design processes, and the recommendations in this report might not be suitable. However, the same evaluation process may still be useful in order to choose the most suitable method. Finally, it should be clarified that even though the selected criteria are relevant and the weighting corresponds to the company's priorities, the method with the highest score is not necessarily the most suitable in all cases. While a Pugh Matrix serves as a tool in the decision making, decisions should not be based solely on the matrix scores.

The methods evaluated in this study is supposed to fill a gap in the early design phase. It is of importance that the methods have a sufficient precision to serve as a guide when making design changes. The methods should give predictions of the right magnitude, as well as capture differences between different designs, but the exact value of the resistance is not important in the early design phase. In later design phases, when the design is set and more accurate predictions may be valuable, the recommendations in this study may not be suitable.

The results from Holtrop & Mennen on Eelex 2020 deviate between 2.2% and 70.6% from the model test results, which is a significantly larger error than 16% shown in a previous study. It can also be concluded that the method has a low precision, and the predictions do not follow a clear pattern. The method is previously shown to be less accurate in cases where the hull geometry is close to the applicability limits, and the fact that the length-beam ratio of Eelex 2020 is below the applicability limit is a possible explanation to the large deviations and low precision. Because Holtrop & Mennen is developed from model tests performed on a number of hulls, the method is only applicable for hull geometries similar to the ones the equations are based on. This is clearly a disadvantage of the method, since it only can be applied when designing hulls with traditional shapes and dimensions. To summarize, Holtrop & Mennen does not provide accurate resistance predictions for Eelex 2020. Despite the low accuracy and precision, Holtrop & Mennen is a quick and user friendly method that does not require neither high competence nor advanced equipment.

The results from Holtrop & Mennen show that the wave resistance is the dominant resistance component as the speed increases. This corresponds well with the theory presented in section 2.1, which states that the pressure resistance, i.e. the wave resistance, increases with increasing speed. This indicates that although Holtrop & Mennen over-estimates the resistance in an inconsistent way, the method seems to capture the theoretical behaviour of the resistance forces. It may therefore be able to apply the method to compare different hull designs, because even though the value of the resistance predictions are inaccurate, it may accurately indicate differences between hull designs. This is however just a speculation, and needs to be confirmed by further investigations.

For low speeds, corresponding to $F_n \leq 0.36$, the CFD results deviate maximum 13.84% from the model test results. The deviations are within acceptable limits, but slightly higher than the 10% error found in previous studies. For 7 and 8 knots, the error is larger, 32.6% and 43.39% respectively. Compared to Holtrop & Mennen, the CFD results are more consistent, especially for the lower speeds in the displacement range. CFD resulted in a total score of 14 in the Pugh Matrix, which is less than half of the total score for Holtrop & Mennen. The drawback with CFD is the time consumption, which is significantly higher than the time for Holtrop & Mennen. However, the time required to perform a CFD simulation covering all speeds simulated in this study takes approximately one week in total time, and three days in active time, excluding the mesh convergence study. The time consumption is considered acceptable and although it is higher than the 30 minutes Holtrop & Mennen takes, one week can be reasonable to spend on resistance predictions. Another aspect influencing the Pugh Matrix outcome is the highly prioritized accessibility, where CFD requires both high competence and suitable hardware and licence, which Holtrop & Mennen does not. If CFD will be applied in-house, X Shore would need to invest in suitable equipment and competence, which might not be an obstacle due to that low cost is not highly prioritized. Once X Shore have equipment and competence, the accessibility will increase. Based on the arguments mentioned above, in combination with the very low precision and accuracy from Holtrop & Mennen, CFD is a more suitable method for X Shore than Holtrop & Mennen, despite the contradictory Pugh Matrix scores. However, the Savitsky method applied for 7 and 8 knots predicts results with better accuracy than both Holtrop & Mennen and CFD.

Compared with the model test results, the Savitsky method under-predicts the results by $20.8\% - 13.7\%$, with an average deviation of 17.18% for the speeds $12 - 32$ knots. The maximum error is for $Fn = 0.72$, which means that although the applicability criteria are fulfilled, the boat has not reached planing and a large error can therefore be expected. It can be seen in figure 23, that although the Savitsky method under-predicts the resistance for the speed range $12 - 32$ knots, the shape of the curve is similar to the curve for model tests. For 7 knots, the Savitsky method over-predicts the resistance with 10.7%, which deviates from the behaviour of the method for the higher speeds. Nevertheless, the Savitsky method provides the most precise results of all applied methods for the speeds that fulfills the applicability criteria of the Savitsky method. The average deviation of the absolute values for the Savitsky method applied to the speeds $7 - 32$ knots is 17.58%. By modifying the method and include a correction factor of 1.1758 the accuracy can be improved, see Appendix F. This correction factor has been added in the developed Python program.

The predicted trim angles from the Savitsky method correspond well with the angles obtained in the model tests, and the error is between 4.8% and 15.3%. The maximum deviation is $0.77°$ and occurs at $Fn = 0.96$. Like Holtrop & Mennen, the Savitsky method is a semi-empirical method based on experiments, and its applicability is limited to hull shapes similar to the ones that the equations are derived from. However, Eelex 2020 fulfills the applicability criteria, which indicates that the method should give acceptable results. Holtrop & Mennen and the Savitsky method have in common that the input values are easily changed, which enables quick adjustments of the hull characteristics and indications of their impact on the resistance. According to section 2.1, LCG should be positioned at $40\% - 45\%$ of the chine length from the transom for displacement hulls, and $25\% - 35\%$ of the chine length for planing hulls. At Eelex 2020, LCG is positioned approximately 40% forward of the transom, which is a good position for displacement, but not optimal for planing speeds. With the flexibility that the Savitsky method offers, LCG can easily be adjusted in order to determine how sensitive the total resistance is to the position. To make a similar study with CFD would take significantly more time and effort.

The CFD simulations for planing speeds vary more than the results from the Savitsky method. While the smallest error is very close to the model test result, only 1.77% deviation at $F_n = 1.44$, the largest error is as much as 40.84% at $F_n = 1.92$. Previous studies show that CFD should yield results with less than 10% error, and that they generally are smaller than the errors from the Savitsky method. The results from this study show the opposite, and one possible explanation is that the ITTC guidelines used are developed for Froude numbers of the order 0.1 and rarely above 1. Thus, above 16 knots, $F_n > 1$ for Eelex 2020, the ITTC guidelines may not be appropriate.

Furthermore, the fact that trim angle is neglected and the running attitude is not accounted for properly, affects the accuracy negatively. According to the Pugh Matrix, the Savitsky method is the most suitable method for resistance predictions in planing speeds, with a total score of 45 compared to 14 for CFD. Due to that CFD both shows lower precision, and requires more time to perform, the recommendation is to apply the Savitsky method for resistance predictions in the planing speed range.

For semi-planing, i.e. $0.4 < F_n < 1$ and speeds $7 - 16$ knots, the running attitude of the hull varies significantly compared to displacement speeds, and consequently the resistance is harder to predict. Since the trim angle has been neglected from the simulations, this might be the explanation to the large deviations of the CFD results, especially for 7 and 8 knots. Possibly, a dynamic mesh which captures the hull motions, and therefore identifies the running attitude, can improve the CFD results in this speed range.

In contrast to the semi-empirical methods, the applicability of CFD is not limited by hull geometry. The limitations for CFD are rather competence and computer capacity. The differences between the results from setup 1 and setup 2 show that the resistance predictions are sensitive to the location of the free surface. Estimating the free surface level accurately requires knowledge of the behaviour of planing hulls, alternatively data from model tests or other methods. For planing speeds, the largest deviation is 40.84% for 32 knots when the free surface location is changed according to model test data. It should be noted that ΔWL is larger for 32 knots than for 20 and 24 knots which could be a source of error. Adjusting the free surface to the same level as for 20 and 24 knots would decrease the error, but the result would probably still be over-estimated. Qualified estimations of the free surface has been proven to be of importance. Another interesting aspect is the effect of a potential implemented trim in the simulations. All the performed simulations in this study are done without any trim, but a trim angle would probably improve the results since it would increase how accurate the running attitude is modelled. Estimating the trim would in the same way as the free surface estimations require a qualified guess, and since the Savitsky method has shown good agreement of the trim angles, a suggestion is to combine CFD and the results of trim angle from the Savitsky method. Combining CFD and the Savitsky method has been tested for 12 and 32 knots, see Appendix F. None of the simulations did converge, and it can be concluded that in order to implement trim in the CFD simulations, at least a new mesh convergence study needs to be conducted.

The selection of methods and models for the CFD simulations is based on theory in chapter 4. However, other methods and models are available and no further investigation regarding the impact of them has been performed. In this study, a mesh convergence study was performed for one Froude number. Consequently, the dimensionless wall distance y^+ is the same in all simulations, which is an inaccurate assumption. To increase the accuracy of the simulations and ensure the quality of the mesh, mesh convergence studies should be made over the whole range of Froude numbers and the value of the dimensionless wall distance should be verified. The blue areas on the hull in figure 20 symbolize air, which may indicate that numerical ventilation occurs. This would decrease the total resistance prediction, but looking at figure 20i for 24 knots, a large area of air in the middle of the hull can be seen. However, the result for 24 knots has the smallest deviation of all simulated speeds, which may indicate that the blue areas have another explanation than numerical ventilation. By checking and adjusting the dimensionless wall distance, the effects from the potential numerical ventilation can be reduced and the overall quality can be improved. Since the y^+ value is supposed to capture the flow close to the hull surface, poor meshing of the boundary layer will affect the total resistance. The fact that the y^+ value has not been checked in this study might explain why the viscous resistance is lower than the pressure resistance, even for low speeds. Another way of increasing the accuracy and quality of the simulation is to change the convergence criteria, i.e. lower the residuals. However, the simulations have shown good convergence and stable solutions with the residuals used in this study, and the quality is assumed to be sufficient in order to determine the suitability of CFD as a method for X Shore.

Besides the possibility to easily evaluate different hulls by simply changing the CAD-file, CFD has a number of advantages. Although the purpose of applying CFD in this study was to predict resistance, the simulations can also predict e.g. pressure distribution on the hull, wave pattern, and turbulence. For that reason, it might be useful in the later design phases and even for higher speeds, if a more complex setup is applied. Additionally, CFD has a lower economical cost than model tests. The major advantage of model tests is that it provides accurate results. Even though it is both costly and time consuming, there are several reasons why it may be useful to perform occasionally, e.g. when predictions with high accuracy are needed. Additionally, model tests can be used to verify and adjust other methods. However, it is not necessary to include model tests in every design process, and if used, it should not be applied in early design phases. As X Shore has a quick manufacturing process and access to the full-scale hulls, another way to validate and adjust the methods is to perform full-scale tests where total resistance and trim angle are measured.

7.1 Conclusion

From the results, it can be concluded that the recommended approach for X Shore to implement in their design process to predict resistance is the Savitsky method for all speeds that fulfils the applicability criteria of the method. If predictions for lower speeds are of interest, CFD is the recommended method. When applying the Savitsky method, it is recommended to follow the procedure in section 6.3 and use the program developed by the authors, where the correction factor has been included. The CFD simulations should be applied according to section 6.4.

8. Future work

One focus for future work should be the mesh used in the CFD simulations. The mesh convergence study have only been conducted for one Froude number, and to improve the accuracy mesh convergence should be checked for all Froude numbers corresponding to speeds between 4 and 32 knots. A suggestion is to perform the CFD simulations with a fixed trim on the hull, in order to determine the sensitivity of the results to changes of the trim angle. It would also be of interest to compare the results from this study with results obtained from simulations performed with a dynamic mesh.

Another improvement that would result in more accurate estimations of the range would be to include appendages in the methods. This requires a re-evaluation of the recommended systematic approach, since it may influence the accuracy of the different methods. To add resistance from appendages in Holtrop & Mennen is straightforward, since the method include it by default. However, for the Savitsky method and CFD, it is more complicated. The Savitsky method does not handle appendages by default and need to be modified. In order to capture the influence from appendages in CFD simulations, appendages need to be properly meshed. Furthermore, the CFD methods and schemes would need to be re-evaluated to be suitable for simulations with appendages.

Even though the semi-empirical methods, and especially Holtrop & Mennen, deviate significantly from model test results, it could be of interest to apply the methods on different hulls and investigate whether it can be used for comparisons of hulls.

References

[1] Statistiska centralbyrån, *Utsläpp av växthusgaser från inrikes transporter efter växthusgas och transportslag. år 1990 - 2018*, 2019. [Online] Available at `http://www.statistikdatabasen.scb.se/pxweb/sv/ssd/START__MI__MI0107/MI0107InTransp/table/tableViewLayout1/` (Accessed 2020-02-19).

[2] Regeringskansliet, *Sverige ska bli ett fossilfritt välfärdsland*, 2018. [Online] Available at `https://www.regeringen.se/artiklar/2018/04/sverige-ska-bli-ett-fossilfritt-valfardsland/` (Accessed 2020-02-19).

[3] P-O. Moksnes, L. Eriander, J. Hansen, J. Albertsson, M. Andersson, U. Bergström, J. Carlström, J. Egardt, R. Fredriksson, L. Granhag, F. Lindgren, K. Nordberg, I. Wendt, S. Wikström, E. Ytreberg, "Fritidsbåtars påverkan på grunda kustekosystem i Sverige", *Havsmiljöinstitutets Rapport 2019:3*, 2019.

[4] E. C. Tupper, *Introduction to naval architecture*. Butterworth-Heinemann, 2013, ISBN: 978-0-08-098237-3.

[5] A. F. Molland, *The Maritime engineering reference book*. Butterworth-Heinemann, 2008, ISBN: 978-0-7506-8987-8.

[6] X Shore, *About X Shore*, 2020. [Online] Available at `https://www.xshore.com/about-x-shore` (Accessed 2020-03-09).

[7] P. Voxakis, "Ship hull resistance calculations using cfd methods", Massachusetts Institute of Technology, 2012.

[8] Z. Zhang, H. Liu, S. Zhu, F. Zhao, "Application of cfd in ship engineering design practice and ship hydrodynamics", *Journal of Hydrodynamics, Ser. B*, vol. 18, no. 3, pp. 315–322, 2006.

[9] K. Garme, "Ship resistance and powering", KTH Center of Naval Architecture, 2012.

[10] D. Frisk and L. Tegehall, "Prediction of high-speed planing hull resistance and running attitude", CHALMERS UNIVERSITY OF TECHNOLOGY, 2015.

[11] J. M. Almeter, "Resistance prediction of planing hulls: State of the art", *Marine Technology*, vol. 30, no. 4, pp. 297–307, 1993.

[12] O. M. Faltinsen, *Hydrodynamics of High-Speed Marine Vehicles*. New York: Cambridge University Press, 2005, ISBN: 978-0-521-84568-7.

[13] A. Kukner and A. Yasa, "High speed planing hulls resistance prediction methods and comparison", Istanbul Technical University, Turkey, 2011.

[14] L. Larsson and R. Eliasson, *Principles of Yacht Design*. International Marine/Ragged Mountain Press; 2 edition, 2000, pp. 183–196, ISBN: 978-0071353939.

[15] L. Birk, *Fundamentals of ship hydrodynamics*. John Wiley & Sons, 2019, ISBN: 978-1-1188-5551-5.

[16] Brusa, "HSM1 - Hybrid Synchronous Motor".

[17] L. Nikolopoulos, E. Boulougouris, "A study on the statistical calibration of the holtrop and mennen approximate power prediction method for full hull form, low froude number vessels", *Journal of Ship Production and Design*, vol. 35, no. 1, pp. 41–68, 2018. DOI: `https://doi.org/10.5957/JSPD.170034`.

[18] International Towing Tank Conference, "Practical guidelines for ship resistance CFD", *ITTC – Recommended Procedures and Guidelines*, vol. 7.5–03–02–04, 2014.

[19] J. Holtrop, G.G.J. Mennen, "An approximate power prediction method", *International Shipbuilding Progress*, vol. 29, no. 335, pp. 166–170, 1982.

[20] D. Savitsky, "Hydrodynamic design of planing hulls", *The Society of Naval Architects and Marine Engineers*, vol. 1, no. 04, 1964.

[21] J. Carlton, *Marine propellers and propulsion*. Butterworth-Heinemann, 2007, ISBN: 978-0-7506-8150-6.

[22] International Towing Tank Conference, "Testing and extrapolation methods, general guidelines for uncertainty analysis in resistance towing tank tests", *ITTC – Recommended Procedures and Guidelines*, vol. 7.5–02–02–02, 2008.

[23] International Towing Tank Conference, "Practical guidelines for ship CFD applications", *ITTC – Recommended Procedures and Guidelines*, vol. 7.5–03–02–03, 2014.

[24] International Towing Tank Conference, "Resistance test", *ITTC – Recommended Procedures and Guidelines*, vol. 7.5–02–02–01, 2011.

[25] F. Çakıcı, Ö.F Sukas, O. Usta, A.D.Alkan, "A computational investigation of a planing hull in calm water by u-ranse approach", International conference on advances in applied and computational mechanics, 2015.

[26] International Towing Tank Conference, "Practical guidelines for ship CFD applications", *ITTC – Recommended Procedures and Guidelines*, vol. 7.5–03–02–03, 2011.

[27] ANSYS Inc., "ANSYS Fluent 12.0 Theory Guide", 2009.

[28] A. Persson, SSPA, [Pesonal communication by e-mail] (2020-02-21).

[29] H. K. Versteeg and W. Malalasekera, *An Introduction to Computation Fluid Dynamics: The Finite Volume Method*. Pearson Education Limited, 2007, ISBN: 9780131274983.

[30] R. A. Bengt Andersson and L. Håkansson, *Computational Fluid Dynamics for Engineers*. Cambridge University Press, 2012, ISBN: 9781139205795.

[31] F. Stern, J. Yang, Z. Wang, H. Sadat-Hosseini, M. Mousaviraad, S. Bhushan, T. Xing, "Computational ship hydrodynamics: Nowadays and way forward", *International Shipbuilding Progress*, vol. 60, no. 1-4, pp. 3–105, 2013. DOI: 10.3233/ISP-130090.

[32] A. Gray-Stephens, T. Tezdogan, S. Day, "Strategies to minimise numerical ventilation in CFD simulations of high-speed planing hulls", *Proceedings of the ASME 2019 38th International Conference on Ocean, Offshore and Arctic Engineering*, 2019.

[33] I. M. Viola, R. G. J. Flay, R. Ponzini, "Cfd analysis of the hydrodynamic performance of two candidate america's cup ac33 hulls", *Transactions of the Royal Institution of Naval Architects Part B: International Journal of Small Craft Technology*, vol. 154, no. 1, B1–B12, 2012. DOI: https://doi.org/10.3940/rina.ijsct.2012.b1.113.

[34] A. Rosén, "Introduction to seakeeping", KTH Center of Naval Architecture, 2011.

[35] ANSYS Inc., "ANSYS Fluent Tutorial Guide", 2017.

[36] ANSYS Inc., "ANSYS Fluent User's Guide", 2013.

[37] NASA, *Evaluating Iterative Convergence*, 2008. [Online] Available at https://www.grc.nasa.gov/WWW/wind/valid/tutorial/iterconv.html (Accessed 2020-02-10).

[38] H. Kerzner, *Project management: a systems approach to planning, scheduling, and controlling*. John Wiley & Sons, 2017, ISBN: 978-1-1191-6537-8.

[39] D. for Communities and L. Government, "Multi-criteria analysis: A manual", Department for Communities and Local Government: London, 2009.

[40] D. S. Burge, "The systems engineering tool box", 2009.

[41] F. S. Stefano Brizzolara, "Accuracy of cfd codes in the prediction of planing surface hydrodynamic characteristics", University of Genoa, Department of Naval Architecture and Marine Technology, Italy, 2007.

[42] J. Zelle, *Graphics.py*, [Online] Available at https://mcsp.wartburg.edu/zelle/python/graphics.py (Accessed 2020-04-06).

[43] J. Holtrop, "A statistical re-analysis of resistance and propulsion data", *International Shipbuilding Progress*, vol. 31, no. 363, pp. 3–5, 1984.

A. Holtrop & Mennen

Nomenclature

A_{BT} = transverse bulb area at the position where the still-water surface intersects the stem
A_M = midships cross-sectional area
A_T = immersed part of the transverse area of the transom at zero speed
A_{WP} = waterplane area
B = maximum breadth
C_A = correlation allowance coefficient
C_B = block coefficient
C_f = friction coefficient
C_M = midship section coefficient
C_P = prismatic coefficient
C_{WP} = waterplane area coefficient
D = average draught
D_AP = draught at aft perpendicular
D_FP = draught at forward perpendicular
F_n = Froude number
F_{ni} = Froude number based on the immersion
F_{nT} = Froude number based on the transom immersion
g = gravitational acceleration
h_B = position of the center of the transverse area A_{BT} above the keel line
lcb = longitudinal position of the center of buoyancy forward of $0.5L$ as percentage of L
L_{WL} = length on waterline
L_R = length of the run
L_{PP} = length between perpendiculars
P_B = coefficient as a measure for the emergence of the bow
R_A = model-ship resistance
R_{APP} = resistance of appendages
R_B = additional pressure resistance of bulbous bow near the water surface
Re = Reynolds number
R_F = frictional resistance according to ITTC formulation
R_{total} = total resistance of a ship
R_{TR} = additional pressure resistance of immersed transom stern
R_W = wave-making and wave-breaking resistance
R_{W-A} = wave-making and wave-breaking resistance for $F_n < 0.4$
R_{W-B} = wave-making and wave-breaking resistance for $F_n > 0.55$
R_{W-C} = wave-making and wave-breaking resistance for $0.4 < F_n < 0.55$
S = wetted surface of the hull
S_{APP} = wetted surface of the appendages
U = ship velocity
$(1 + k_1)$ = form factor describing the viscous resistance of the hull form in relation to R_F
$(1 + k_2)$ = appendage resistance factor
∇ = volume displacement
ν = kinematic viscosity
ρ = density of the fluid

If nothing else is specified, the equations in this appendix come from Holtrop & Mennen [19].

The total resistance is subdivided into

$$R_{total} = R_F(1 + k_1) + R_{APP} + R_W + R_B + R_{TR} + R_A \tag{A.1}$$

and is determined by the following steps.

Step 1:
The first term, R_F is the frictional resistance according to the ITTC formulation [18]

$$R_F = \frac{1}{2}\rho U^2 C_f S \tag{A.2}$$

where ρ is the density of the water, U is the speed of the boat and S is the wetted surface of the hull. C_f is the friction coefficient [23] defined as

$$C_f = \frac{0.075}{[log_{10}(Re) - 2]^2} \tag{A.3}$$

where Re is the Reynolds number defined as

$$Re = \frac{UL_{PP}}{\nu} \tag{A.4}$$

where L_{PP} is the length between perpendiculars and ν is the kinematic viscosity [22].

The wetted surface of the hull can be approximated as

$$\begin{aligned} S =& L_{WL}(2D + B)\sqrt{(C_M)}(0.453 + 0.4425C_B - 0.2862C_M \\ & - 0.003467\left(\frac{B}{D}\right) + 0.3696C_{WP}) + 2.38\left(\frac{A_{BT}}{C_B}\right) \end{aligned} \tag{A.5}$$

where L_{WL} is the waterline length, B is the maximum breadth and A_{BT} is the transverse sectional area of the bulb at the position where the still-water intersects the stem. The average draught D is defined as

$$D = \frac{D_{FP} + D_{AP}}{2} \tag{A.6}$$

where D_{FP} is the draught at the forward perpendicular and D_{AP} is the draught at the aft perpendicular of the hull. C_M is the midship section coefficient, C_B is the block coefficient and C_{WP} is the waterplane area coefficient defined as

$$C_M = \frac{A_M}{BD} \tag{A.7}$$

$$C_B = \frac{\nabla}{L_{PP}BD} \tag{A.8}$$

$$C_{WP} = \frac{A_{WP}}{LB} \tag{A.9}$$

where A_M is the immersed midship sectional area at $L_{WL}/2$, ∇ is the displacement volume and A_{WP} is the waterplane area [9].

Step 2:
The frictional resistance is multiplied with a form factor $(1 + k_1)$ describing the viscous resistance of the hull form in relation to R_F. The form factor is defined as

$$(1 + k_1) = c_{13}(0.93 + c_{12}\left(\frac{B}{L_R}\right)^{0.92497}(0.95 - C_P)^{-0.521448}(1 - C_P + 0.0225lcb)^{0.6906}) \tag{A.10}$$

where lcb is the longitudinal position of the center of buoyancy forward of $0.5L_{WL}$ as a percentage of L_{WL}. The prismatic coefficient C_P is based on L_{PP} and defined as [9]

$$C_P = \frac{\nabla}{L_{PP}A_M} \tag{A.11}$$

In the form factor formula, L_R is a parameter reflecting the length of the run and is defined as

$$L_R = L_{WL}\left(\frac{1 - C_P + 0.06C_Plcb}{4C_P - 1}\right) \tag{A.12}$$

The form factor does also contain two coefficients, c_{12} and c_{13}. The first one is defined as

$$c_{12} = \begin{cases} \left(\frac{D}{L_{WL}}\right)^{0.2228446} & \text{when } \left(\frac{D}{L_{WL}}\right) > 0.05 \\ 48.20\left(\frac{D}{L_{WL}} - 0.02\right)^{2.078} + 0.479948 & \text{when } 0.02 < \left(\frac{D}{L_{WL}}\right) < 0.05 \\ 0.479948 & \text{when } \left(\frac{D}{L_{WL}}\right) < 0.02 \end{cases} \tag{A.13}$$

The other coefficient c_{13} is defined as

$$c_{13} = 1 + 0.003C_{stern} \tag{A.14}$$

and accounts for the specific shape of the afterbody related to the coefficient C_{stern} which have the tentative guidelines presented in table A.1.

Table A.1: Tentative guidelines for the specific shape of the afterbody of the ship.

Afterbody form	C_{stern}
V-shaped sections	-10
Normal section shape	0
U-shaped sections with Hogner stern	+10

Step 3:
The appendage resistance is the next term in the total resistance formulation and it is defined as

$$R_{APP} = 0.5\rho U^2 S_{APP}(1 + k_2)_{eq} C_f \tag{A.15}$$

where S_{APP} is the wetted surface of the appendages and $(1 + k_2)$ is the appendage resistance factor. Tentative values for the factor $(1 + k_2)$ are presented in table A.2, obtained from resistance tests with bare and appended ship models.

Table A.2: Tentative values for the appendage resistance factor $(1 + k_2)$.

Approximate $(1 + k_2)$ values	
Rudder behind skeg	1.5 - 2.0
Rudder behind stern	1.3 - 1.5
Twin-screw balance rudders	2.8
Shaft brackets	3.0
Skeg	1.5 - 2.0
Strut bossings	3.0
Hull bossings	2.0
Shafts	2.0 - 4.0
Stabilizer fins	2.8
Dome	2.7
Bilge keels	1.4

A combination of appendages is determined as

$$(1+k_2)_{eq} = \frac{\sum(1+k_2)S_{APP}}{\sum S_{APP}} \tag{A.16}$$

Step 4:
Following, the wave resistance R_W is depending on the Froude number F_n, based on the waterline length L_{WL} and defined as

$$F_n = \frac{U}{\sqrt{gL_{WL}}} \tag{A.17}$$

For the speed range $F_n < 0.4$, the wave resistance is defined as

$$R_{W-A} = c_1 c_2 c_5 \nabla \rho g e^{(m_1 F_n^d + m_4 cos(\lambda F_n^{-2}))} \tag{A.18}$$

and for the speed range $F_n > 0.55$ the wave resistance is defined as

$$R_{W-B} = c_{17} c_2 c_5 \nabla \rho g e^{(m_3 F_n^d + m_4 cos(\lambda F_n^{-2}))} \tag{A.19}$$

where c_1, c_2, c_5, c_{17}, m_1, m_3, m_4 and λ are coefficients, g is the gravitational acceleration and $d = -0.9$. [43] [19] For the speed range $0.4 < F_n < 0.55$ the wave resistance is defined as

$$R_{W-C} = R_{W-A_{0.4}} + \frac{(10F_n - 4)(R_{W-B_{0.55}} - R_{W-A_{0.4}})}{1.5} \tag{A.20}$$

which is an interpolation formula where $R_{W-A_{0.4}}$ is the wave resistance for $F_n = 0.4$ and $R_{W-B_{0.55}}$ is the wave resistance for $F_n = 0.55$ according to equation A.18 and A.19 respectively [43].

The first coefficient c_1 is determined as

$$c_1 = 2223105 c_7^{3.78613} \left(\frac{D}{B}\right)^{1.07961} (90 - i_E)^{-1.37565} \tag{A.21}$$

and

$$c_7 = \begin{cases} 0.229577 \left(\frac{B}{L_{WL}}\right)^{0.33333} & \text{when } \left(\frac{B}{L_{WL}}\right) < 0.11 \\ \frac{B}{L_{WL}} & \text{when } 0.11 < \left(\frac{B}{L_{WL}}\right) < 0.25 \\ 0.5 - 0.0625 \left(\frac{L_{WL}}{B}\right) & \text{when } \left(\frac{B}{L_{WL}}\right) > 0.25 \end{cases} \tag{A.22}$$

The angle of the waterline at the bow in degrees with reference to the center plane is called the half angle of entrance, i_E, neglecting the local shape at the stem. If this angle is unknown, it can be determined as

$$i_E = 1 + 89 e^{\left(-\left(\frac{L}{B}\right)^{0.80856} (1-C_{WP})^{0.30484} (1-C_P-0.0225lcb)^{0.6367} \left(\frac{L_R}{B}\right)^{0.34574} \left(\frac{100\nabla}{L_{WL}^3}\right)^{0.16302}\right)} \tag{A.23}$$

The second coefficient c_2 accounts for the reduction of the wave resistance due to the action of a bulbous bow and is defined as

$$c_2 = e^{(-1.89\sqrt{c_3})} \tag{A.24}$$

where the coefficient determining the influence of the bulbous bow on the wave resistance is defined as

$$c_3 = \frac{0.56 A_{BT}^{1.5}}{BD(0.31\sqrt{A_{BT}} + D_{FP} - h_B)} \tag{A.25}$$

where h_B is the position of the center of the transverse area A_{BT} above the keel line. Next coefficient express the influence of a transom stern on the wave resistance and is defined as

$$c_5 = \frac{1 - 0.8 A_T}{BDC_M} \tag{A.26}$$

where A_T is the immersed part of the transverse area of the transom at zero speed. Following, c_{17} is defined as [43]

$$c_{17} = 6919.3 C_M^{-1.3346} \left(\frac{\nabla}{L_{WL}^3}\right)^{2.00977} \left(\frac{L_{WL}}{B} - 2\right)^{1.40692} \tag{A.27}$$

The remaining coefficients m_1, m_3, m_4 and λ are determined as follows [43] [19]

$$m_1 = 0.0140407 \left(\frac{L_{WL}}{D}\right) - 1.75254 \left(\frac{\nabla^{1/3}}{L_{WL}}\right) - 4.79323 \left(\frac{B}{L_{WL}}\right) - c_{16} \tag{A.28}$$

where

$$c_{16} = \begin{cases} 8.07981 C_P - 13.8673 C_P^2 + 6.984388 C_P^3 & \text{when } C_P < 0.80 \\ 1.73014 - 0.7067 C_P & \text{when } C_P > 0.80 \end{cases} \tag{A.29}$$

$$m_3 = -7.2035 \left(\frac{B}{L_{WL}}\right)^{0.326869} \left(\frac{D}{B}\right)^{0.605375} \tag{A.30}$$

$$m_4 = c_{15} 0.4 e^{(-0.034 F_n^{-3.29})} \tag{A.31}$$

where

$$c_{15} = \begin{cases} -1.69385 & \text{when } \frac{L_{WL}^3}{\nabla} < 512 \\ -1.69385 + \frac{\frac{L_{WL}}{\nabla^{1/3}} - 8.0}{2.36} & \text{when } 512 < \frac{L_{WL}^3}{\nabla} < 1727 \\ 0.0 & \text{when } \frac{L_{WL}^3}{\nabla} > 1727 \end{cases} \tag{A.32}$$

and

$$\lambda = \begin{cases} 1.446 C_P - 0.03 \left(\frac{L_{WL}}{B}\right) & \text{when } \frac{L_{WL}}{B} < 12 \\ 1.446 C_P - 0.36 & \text{when } \frac{L_{WL}}{B} > 12 \end{cases} \tag{A.33}$$

Step 5:
The additional resistance R_B due to the presence of a bulbous bow near the surface is defined as

$$R_B = \frac{0.11 e^{(-3 P_B^{-2})} F_{ni}^3 A_{BT}^{1.5} \rho g}{1 + F_{ni}^2} \tag{A.34}$$

where P_B is the coefficient of the measure for the emergence of the bow defined as

$$P_B = \frac{0.56\sqrt{A_{BT}}}{D_{FP} - 1.5h_B} \tag{A.35}$$

and F_{ni} is the froude number based on the immersion determined as

$$F_{ni} = \frac{U}{\sqrt{g(D_{FP} - h_B - 0.25\sqrt{A_{BT}}) + 0.15U^2}} \tag{A.36}$$

Step 6:
The additional pressure resistance R_{TR} due to the immersed transom is defined as

$$R_{TR} = 0.5\rho U^2 A_T c_6 \tag{A.37}$$

where

$$c_6 = \begin{cases} 0.2(1 - 0.2F_{nT}) & \text{when } F_{nT} < 5 \\ \\ 0 & \text{when } F_{nT} \geq 5 \end{cases} \tag{A.38}$$

related to the Froude number based on the transom immersion

$$F_{nT} = \frac{U}{\sqrt{\frac{2gA_T}{B + BC_{WP}}}} \tag{A.39}$$

Step 7:
The last contribution to the total resistance is the model-ship correlation resistance R_A is supposed to describe primarily the effect of the hull roughness and the still-air resistance. It is defined as

$$R_A = \frac{1}{2}\rho U^2 S C_A \tag{A.40}$$

where C_A is the correlation allowance coefficient based on results of speed trials

$$C_A = 0.006(L_{WL} + 100)^{-0.16} - 0.00205 + 0.003\sqrt{\frac{L_{WL}}{7.5}}C_B^4 c_2 (0.04 - c_4) \tag{A.41}$$

where

$$c_4 = \begin{cases} \frac{D_{FP}}{L_{WL}} & \text{when } \frac{D_{FP}}{L_{WL}} \leq 0.04 \\ \\ 0.04 & \text{when } \frac{D_{FP}}{L_{WL}} > 0.04 \end{cases} \tag{A.42}$$

B. Savitsky method

Nomenclature

a = distance between the viscous drag component D_f and the center of gravity, measured normal to D_f
B = beam of the boat
c = the distance between the center of pressure and the center of gravity, measured parallel to the keel
C_f = friction coefficient
C_{L0} = lift coefficient
$C_{L\beta}$ = planing coefficient
C_p = center of pressure
C_V = planing coefficient
D = total drag
D_f = viscous drag component
f = distance between the propeller axis and the center of gravity, measured normal to the propeller axis
g = gravitational acceleration
LCG = longitudinal center of gravity measured along the keel from the transom
Re = Reynolds number
U = ship velocity
U_1 = speed at the hull bottom
VCG = vertical center of gravity measured from the keel line
β = deadrise angle
γ = specific weight of water
Δ = displacement mass of the boat
ϵ = the inclination of the propeller axis relative to the keel
Λ = mean wetted length-beam ratio
ν = kinematic viscosity
ρ = density of water
τ = trim angle
$\varphi = \gamma/g$

If nothing else is specified, the equations in this appendix come from Savitsky [20].

Note that all input values must be expressed in imperial units, and *not* SI-units.

Step 1:
Calculate the planing coefficients C_V and $C_{L\beta}$:

$$C_V = \frac{U}{\sqrt{(gB)}} \tag{B.1}$$

$$C_L\beta = \frac{\Delta}{\frac{1}{2}\varphi U^2 B^2} \tag{B.2}$$

where g is the gravitational acceleration, B is the beam of the boat, Δ is the displacement, U is the speed of the boat and φ is defined as

$$\varphi = \frac{\gamma}{g} \tag{B.3}$$

where γ is the specific weight of water.

Step 2:
Making the following steps for a number of different values of τ will enable solving a moment equation and through linear interpolation finding the equilibrium trim angle.

Solve for C_{L0}:

$$C_{L\beta} = C_{L0} - 0.0065\beta C_{L0}^{0.60} \tag{B.4}$$

where β is the deadrise angle. The mean wetted length-beam ratio Λ is determined by solving following equation for Λ:

$$C_{L0} = \tau^{1.1} \left(\frac{0.0120\Lambda^{1/2} + 0.0055\Lambda^{5/2}}{{C_V}^2} \right) \tag{B.5}$$

The speed at the hull bottom U_1 differs from the speed of the boat U and is approximated to

$$U_1 = 0.95U \tag{B.6}$$

Reynold's number is calculated by

$$Re = \frac{U_1 \Lambda B}{\nu} \tag{B.7}$$

where ν is the kinematic viscosity of water. The frictional coefficient is calculated according to ITTC [23] and defined as

$$C_f = \frac{0.0075}{[log_{10}(Re) - 2]^2} \tag{B.8}$$

The viscous component of drag D_f is defined as

$$D_f = \frac{\varphi {U_1}^2 \Lambda B^2 (C_f + \Delta C_f)}{2cos(\beta)} \tag{B.9}$$

where $\Delta C_f = 0.0004$ according to ATTC standard. The total drag D can then be calculated by

$$D = \Delta tan(\tau) + \frac{\varphi {U_1}^2 \Lambda B^2 (C_f + \Delta C_f)}{2cos(\beta)cos\tau} \tag{B.10}$$

The center of pressure C_p can be calculated as

$$C_p = 0.75 - \frac{1}{\frac{5.21 C_V^2}{\Lambda^2} + 2.39} \tag{B.11}$$

and is needed to determine the distance between the center of pressure and the center of gravity, measured parallel to the keel:

$$c = LCG - C_p \Lambda B \tag{B.12}$$

where LCG is the longitudinal center of gravity measured along the keel from the transom. The distance between the viscous component of drag D_f and the center of gravity, measured normal to D_f is defined as

$$a = VCG - \frac{b}{4} tan\beta \tag{B.13}$$

where VCG is the vertical center of gravity measured from the keel line. Finally, the momentum equation that should be fulfilled in order to obtain the equilibrium trim angle is

$$\Delta \left(\frac{(1 - sin(\tau) sin(\tau + \epsilon))c}{cos\tau} - f sin\tau \right) + D_f (a - f) = 0 \tag{B.14}$$

where ϵ is the inclination of the propeller axis relative to the keel and f is the distance between the propeller axis and the center of gravity, measured normal to the propeller axis.

Step 3:
When equation B.14 has been calculated for different values of τ, i.e $f(\tau)$, linear interpolation can be used to find the equilibrium trim angle τ_{eq} that fulfills the equation.

$$\tau_{eq} = \tau_1 - f(\tau_1)\left(\frac{\tau_2 - \tau_1}{f(\tau_2) - f(\tau_1)}\right) \tag{B.15}$$

Step 4:
When the equilibrium trim angle τ_{eq} is identified, equations B.5-B.9 need to be calculated again, with τ_{eq}. Finally, by using the obtained values in

$$D = \Delta tan(\tau_{eq}) + \frac{\varphi {U_1}^2 \Lambda_{eq} B^2 (C_{f\,eq} + \Delta C_f)}{2cos(\beta)cos\tau_{eq}} \tag{B.16}$$

the total resistance is evaluated. The index eq means that the value is calculated with the equilibrium trim angle τ_{eq}, and τ_1 and τ_2 should be chosen so that $f(\tau_1) < 0$ and $f(\tau_2) > 0$. The unit of D is pound-force, lbf, and can be converted to newton:

$$D_N = 9.81\frac{D}{2.205} \tag{B.17}$$

C. Program interface for Holtrop & Mennen

Figure C.1 shows the input window in the Python program developed for Holtrop & Mennen. The output window is presented in figure C.2.

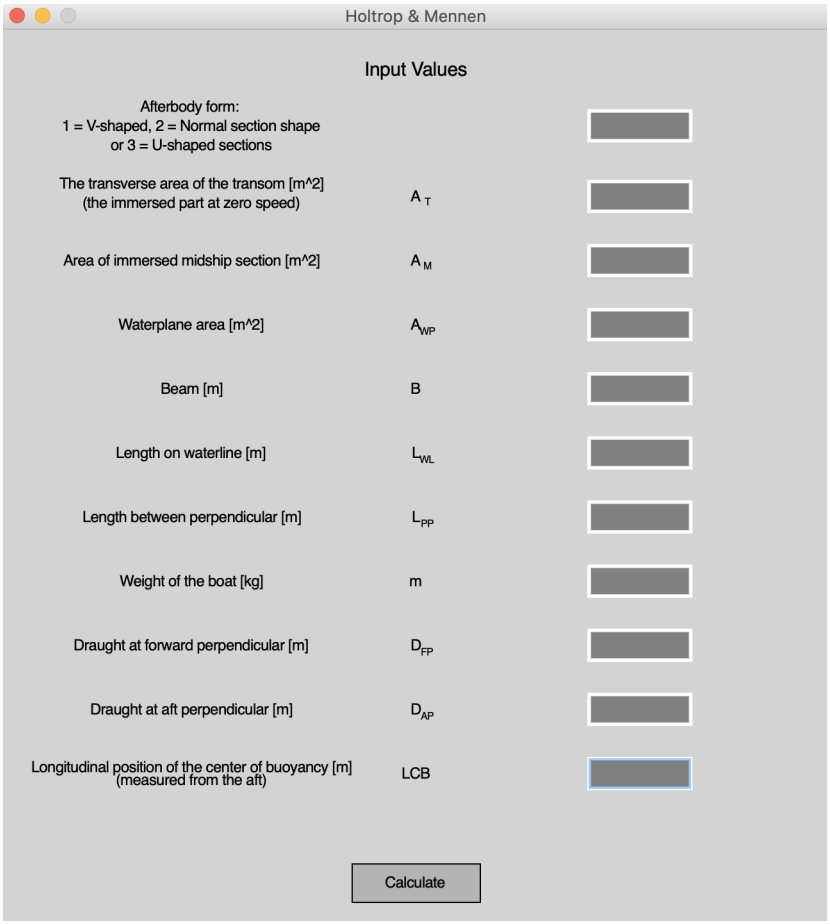

Figure C.1: User interface of Holtrop & Mennen program.

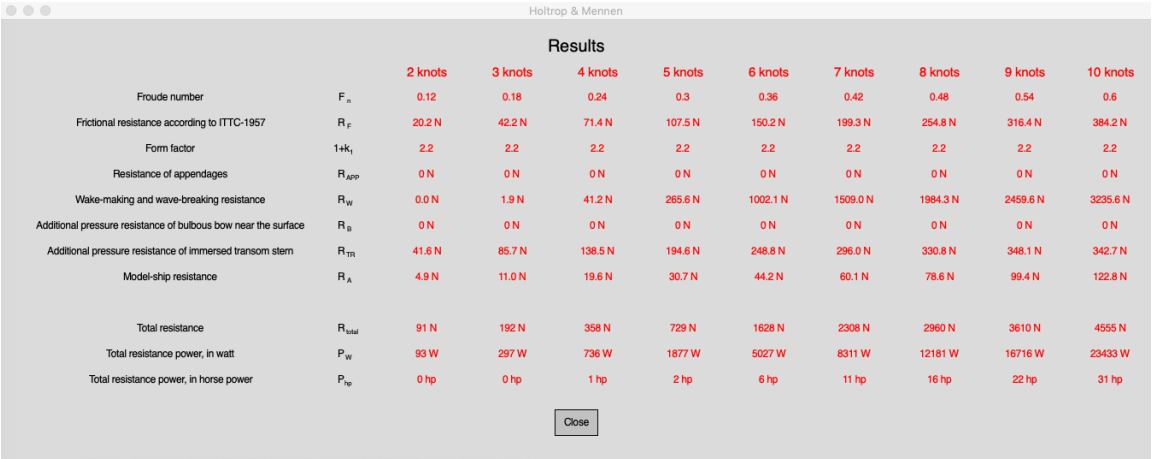

Figure C.2: The results from applying Holtrop & Mennen on Eelex 2020.

D. Program interface for the Savitsky method

Figure D.1 shows the input window in the Python program developed for the Savitsky method. The output window is presented in figure D.2.

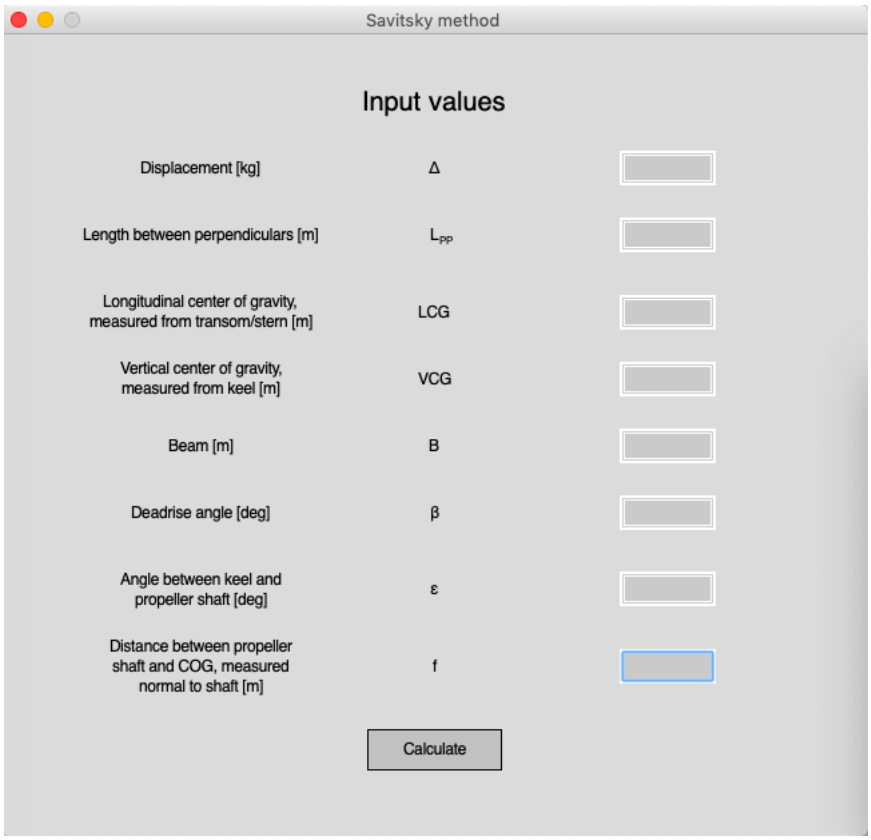

Figure D.1: User interface of the Savitsky program.

Figure D.2: The results from applying the Savitsky method on Eelex 2020.

E. Results

Table E.1 presents the resulting resistance force from applying model tests, Holtrop & Mennen, CFD and the Savitsky method on Eelex 2020 in displacement speeds $4 - 8$ knots.

Table E.1: Resulting resistance force from applying model tests, Holtrop & Mennen, CFD and the Savitsky method on Eelex 2020 in displacement speeds.

	4 knots	**5 knots**	**6 knots**	**7 knots**	**8 knots**
Froude number	0.24	0.30	0.36	0.42	0.48
Model tests	350 N	613 N	954 N	1497 N	2268 N
Holtrop & Mennen	358 N	729 N	1628 N	2308 N	2960 N
CFD	390 N	542 N	822 N	1014 N	1284 N
Savitsky	-	-	-	1657 N	1823 N

Table E.2 presents the resulting resistance force from applying model tests, the Savitsky method and CFD on Eelex 2020 in semi-planing and planing speeds $12 - 32$ knots. Table E.3 and E.4 present the resulting trim angle and the difference in trim angle from model tests and the Savitsky method.

Table E.2: Resulting resistance from applying model tests, the Savitsky method, and CFD on Eelex 2020 in planing speeds.

	12 knots	**16 knots**	**20 knots**	**24 knots**	**32 knots**
Froude number	0.72	0.96	1.20	1.44	1.92
Model tests	3290 N	3831 N	3916 N	4286 N	5713 N
Savitsky	2604 N	3114 N	3379 N	3690 N	4641 N
CFD	2596 N	3268 N	3144 N	4362 N	8046 N

Table E.3: Resulting trim angles from applying model tests and the Savitsky method on Eelex 2020 in planing speeds.

	7 knots	**8 knots**	**12 knots**	**16 knots**	**20 knots**	**24 knots**	**32 knots**
Froude number	0.42	0.48	0.72	0.96	1.20	1.44	1.92
Model tests	1.43°	2.80°	4.17°	5.04°	4.28°	3.52°	2.56°
Savitsky	2.88°	3.04°	3.97°	4.27°	3.81°	3.23°	2.37°

Table E.4: Difference in trim angle in percentage between model tests and Savitsky.

	7 knots	**8 knots**	**12 knots**	**16 knots**	**20 knots**	**24 knots**	**32 knots**
Froude number	0.42	0.48	0.72	0.96	1.20	1.44	1.92
Savitsky	101.4%	8.57%	−4.8%	−15.3%	−11.0%	−8.2%	−7.4%

F. Modifying and combining methods

F.1 Modifying the Savitsky method with a correction factor

By adding a correction factor of 1.1758 to the total resistance from the Savitsky method, the accuracy of the method is improved, see figure F.1.

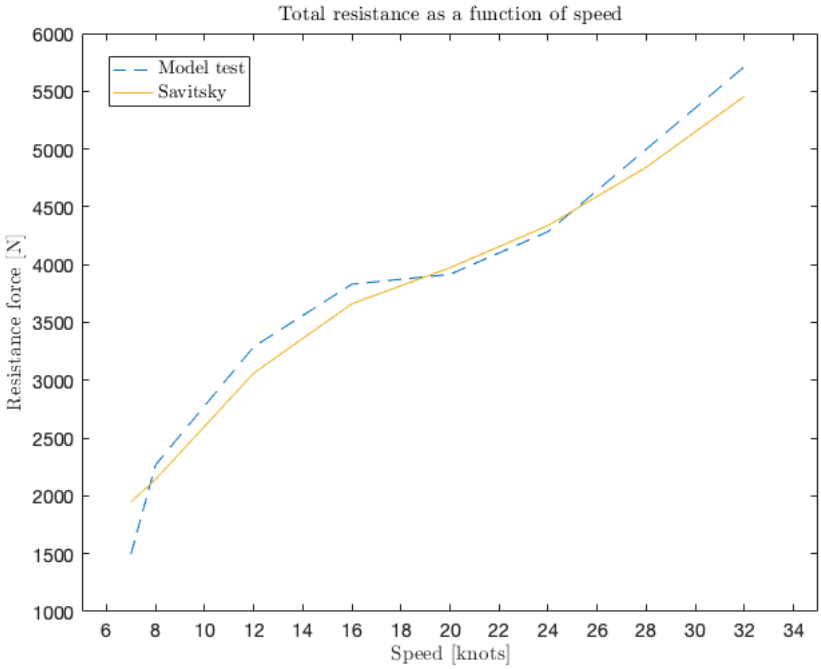

Figure F.1: Resulting resistance force from the modified Savitsky method compared to the model tests for Eelex 2020.

F.2 Combining CFD and the Savitsky method

The estimated values for trim angles and draught from the Savitsky method were used in the CFD simulations in order to investigate if the accuracy of the resistance predictions could be improved. The trim angle was implemented in the CAD file, where the hull was rotated around the coordinate system. The same computational domain, mesh and setup as in the simulations without trim angles were used. The free surface was located to generate a draught at transom corresponding to the values presented in table F.1. The simulations were made for two different speeds, 12 knots and 32 knots.

Table F.1: Values used in the CFD simulations with trim angles.

Speed	**Trim angle**	**Draught at transom**	**Converged**
12 knots	3.97°	0.55 m	No
32 knots	2.37°	0.28 m	No

None of the simulations with implemented trim converged, and for 32 knots, an error indicating a too coarse mesh appeared. To combine CFD and the Savitsky method, another mesh and/or setup is required.

TRITA TRITA-SCI-GRU 2020:185